Received: 21 October 2024 | Revised: 10 February 2025 | Accepted: 10 February 2025

DOI: 10.1002/alz.70077

Alzheimer's & Dementia®
THE JOURNAL OF THE ALZHEIMER'S ASSOCIATION

RESEARCH ARTICLE

Fibrillar tau alters cerebral endothelial cell metabolism, vascular inflammatory activation, and barrier function in vitro and in vivo

Roberto Guzmán-Hernández | **Silvia Fossati**

Alzheimer's Center at Temple, Department of Neural Sciences, Temple University Lewis Katz School of Medicine, Philadelphia, Pennsylvania, USA

Correspondence
Silvia Fossati, Alzheimer's Center at Temple, Department of Neural Sciences, Temple University Lewis Katz School of Medicine, 3500 North Broad Street, MERB-647 Philadelphia, PA 19140, USA.
Email: silvia.fossati@temple.edu

Funding information
NIH, Grant/Award Numbers: R01NS104127, R01AG062572; Pennsylvania Department of Health Collaborative Research on Alzheimer's Disease (PA Cure); Pennsylvania Department of Health; National Institute of Neurological Disorders and Stroke, Grant/Award Number: R01NS104127; National Institute on Aging, Grant/Award Number: R01AG062572

Abstract

INTRODUCTION: The presence of tau aggregates in and around the brain vasculature in Alzheimer's disease (AD) and tauopathies suggests its possible pathogenicity to cerebral endothelial cells (ECs).

METHODS: We used an in vitro model of the blood–brain barrier (BBB) to understand the mechanisms of fibrillar tau–mediated cerebral EC and BBB pathology, confirming our findings in 3-month-old P301S mice brains and extracted microvessels.

RESULTS: Protofibrillar and fibrillar tau species induce endothelial barrier permeability through an increase in glycolysis, which activates ECs toward a pro-inflammatory phenotype, inducing loss of junction protein expression and localization. The Warburg-like metabolic shift toward glycolysis and increased vascular pathological phenotypes are also present in young P301S mice.

DISCUSSION: In sum, our work reveals that fibrillar tau species, by enhancing endothelial glycolytic metabolism, promote vascular inflammatory phenotypes and loss of BBB function, highlighting the importance of addressing and targeting early tau-mediated neurovascular damage in AD and tauopathies.

KEYWORDS
Alzheimer's disease, blood–brain barrier, endothelial cells, fibrils, glycolysis, junction protein, mitochondria, neuroinflammation, tau, tauopathies

Highlights

- We improve the understanding of the mechanisms of vascular pathology in tauopathies.
- Fibrillar tau mediates vascular metabolic changes, inflammation, and blood–brain barrier (BBB) dysfunction.
- These events are replicated at early stages in a tauopathy mouse model.
- Inhibiting altered glycolysis reduces BBB permeability and endothelial activation.

1 | BACKGROUND

Cerebrovascular dysfunction and alterations of the neurovascular unit (NVU) have been highlighted as early pathologies, causal to cognitive decline in neurodegenerative diseases and particularly in Alzheimer's disease (AD).[1,2] The NVU is a complex system composed of several cell types, including endothelial cells (ECs), pericytes, smooth muscle cells, glial cells, and neurons, working in concert to regulate blood–brain barrier (BBB) function, neuroinflammation, and neurovascular coupling.[3] The NVU tightly regulates cerebral blood flow, nutrient availability, energy homeostasis, and overall brain functionality. It has been established that the accumulation of amyloid beta (Aβ) around blood vessels, known as cerebral amyloid angiopathy (CAA), present in ≈ 90% of AD cases, has toxic effects on ECs, on the BBB, and on the NVU.[4–7]

Recent studies have highlighted the presence of tau species localized at the brain vascular walls in AD and other neurological disorders,[8–14] such as traumatic brain injury[15] and chronic traumatic encephalopathy.[16,17] Pathological tau can also induce progressive alterations in vessel morphology in aged tauopathy mice,[11] and tau depletion was shown to prevent BBB damage in an inducible tauopathy mouse model.[12] Most recently, it has been reported that oligomeric tau entry into brain ECs induces senescence phenotypes, leading to microvascular dysfunction.[9] Physiologically, tau regulates neuronal microtubule stability in a balanced phosphorylation/dephosphorylation state. Under pathological conditions, hyperphosphorylated tau detaches from microtubules resulting in cytoskeletal instability, impaired intracellular transport, synaptic loss, and cell death. Hyperphosphorylated tau is prone to progressive aggregation into soluble oligomers, protofibrils, fibrils, paired helical filaments (PHFs), and eventually neurofibrillary tangles (NFTs). Intermediate aggregation species of tau, such as oligomers or protofibrils, have been shown to be toxic for neuronal cells.[18] These tau misfolded[19] species are also understood to move throughout the brain through a process known as tau spreading, transmission, or seeding.[8,20] Hence, aggregated tau species, mainly produced in neurons and astrocytes, may reach ECs and the brain vasculature, particularly via astrocytic end feet or neuronal processes,[9,13] which actively communicate with ECs at the NVU. Several receptors have been identified to participate in tau spreading, yet aggregated extracellular tau can also be internalized through endocytosis.[20–25] However, while tau aggregates are known to promote neuronal damage and cell death, the mechanistic contribution of tau aggregated species to endothelial and cerebrovascular dysfunction remains greatly understudied.

ECs form the semi-permeable BBB and are known to regulate neuroinflammation and nutrient availability in the brain.[4,26] Brain ECs are connected to each other by adherent and tight junction proteins (JPs), such as cadherins, occludins, and claudins. which are also linked to the cytoskeleton, regulating EC morphology and structure.[27,28] During activation due to inflammation or vascular permeability, ECs express specific adhesion molecules, such as vascular cell adhesion molecule 1 (VCAM-1) and intercellular adhesion molecule 1 (ICAM-1), to facilitate immune cell infiltration into the brain parenchyma, thus mediating BBB permeability and neuroinflammation.

Peripheral ECs produce most of their energy requirements through glycolysis and contain between 2% and 6% mitochondria by cytoplasmic volume.[29–31] Endothelial mitochondria are thus understood to function primarily as signaling hubs and integrators of environmental stimuli.[32] Remarkably, however, brain ECs contain ≈ 8% to 11% mitochondria per cytoplasmic volume, suggesting a more crucial role for mitochondrial adenosine triphosphate (ATP) production at the BBB. Mitochondrial signaling in ECs, through reactive oxygen species, ATP, Ca^{2+}, and mitochondrial DNA, regulates several cellular processes, such as inflammation, angiogenesis, responses to hypoxia, and cell death.[4,6,33] Moreover, a metabolic shift to glycolysis has been tightly linked to endothelial inflammatory activation.[26,30,34–37]

Although cerebrovascular disease is greatly associated with the onset and progression of AD, the molecular and metabolic mechanisms through which pathological tau species affect endothelial and BBB functionality remain severely understudied.[38–40] In this study, we elucidate molecular changes in endothelial metabolism and inflammatory activation instigated by fibrillar and protofibrillar tau species to mediate EC dysfunction and loss of barrier function, which may contribute to NVU dysfunction and precipitate neurodegeneration in AD and other tauopathies.

RESEARCH IN CONTEXT

1. **Systematic review**: Recent literature highlights the presence of tau in and around the human cerebral vasculature in AD, as also observed in tauopathy mouse models. Senescence and inflammatory phenotypes have been identified as oligomeric tau-mediated pathologies in cerebral endothelial cells (ECs). No previous studies have examined how endothelial metabolic function and barrier pathology are influenced by fibrillar tau species.
2. **Interpretation**: Our results reinforce that tau induces pro-inflammatory phenotypes in brain ECs as an early event that contributes to eventual neurovascular pathology. This study further links an increased glycolytic endothelial metabolism to barrier function impairment; specifically, an increase in glycolysis is associated to endothelial activation and loss of junction protein localization and function.
3. **Future directions**: This work states the importance of understanding metabolic alterations as early mediators of brain vascular pathology in Alzheimer's disease and tauopathies and suggests the need for further studies to clarify the mechanisms of tau-mediated cerebrovascular toxicity.

2 | MATERIALS AND METHODS

2.1 | Preparation of tau aggregates

Monomeric 1N4R tau (Recombinant Human Tau 412; R&D Systems, SP-501) was pre-aggregated into fibrillar species as in Mutreja and Gamblin.[41] Briefly, tau monomers were incubated overnight at 25°C in a solution containing: 5 mM dithiothreitol, pH 8.0; 200 mM NaCl; 10 mM HEPES, pH 7.64; 0.1 mM ethylenediaminetetraacetic acid (EDTA), pH8.0; and 75 μM arachidonic acid (Millipore Sigma 181198). The resulting 2 μM protofibrillar tau stock was further diluted in endothelial basal media 2 (EBM-2) supplemented with 1% fetal bovine serum (FBS) at the required concentrations, for cell culture experimental procedures. Human tau-seeded fibrils were obtained as courtesy of Dr. Rakez Kayed (University of Texas Medical Branch) and prepared as previously published[42,43] (see Supplementary Protocol in supporting information).

2.2 | Electron microscopy

Carbon-coated 400-mesh copper grids (Electron Microscopy Sciences) were glow discharged using a PELCO easiGlow Glow Discharge Cleaning System. Aliquots (10 μL) of the 2 μM protofibrillar 1N4R tau stock were placed onto previously glow-discharged grids, then negative stained with 1% filtered uranyl acetate in distilled water. Stained grids were examined using a AMT BioSprint 12, 12 MP bottom-mounted charge-coupled device camera and AMT software (MitoCare Service Center, Thomas Jefferson University).

2.3 | Cell culture

Immortalized human cerebral microvascular endothelial cells (hCMECs/D3), shown to maintain characteristics of the BBB, were obtained from Babette Weksler (Cornell University).[44] Cells were grown in EBM-2 (Lonza) supplemented with 5% FBS and growth factors (hydrocortisone, hFGF-B, VEGF, R3-IGF-1, ascorbic acid, hEGF, and GA-1000) and maintained in a humidified cell culture incubator under a 5% CO_2 atmosphere at 37°C. Primary human cerebral endothelial cells (hCECs; ScienCell) used for the JP staining, were maintained under the same conditions, and used for < 6 passages. All experimental treatments were prepared in EBM-2 containing 1% FBS, including: pre-aggregated 1N4R tau fibrils, tau monomers, the arachidonic acid–containing vehicle, human IL-4 antibody (R&D Systems, MAB304; αIL-4, 1:100), heptelidic acid (abcam, ab144269, 100 nM), 2-deoxyglucose (Sigma D8375, 1 mM), and human tau fibrils.[42] Cells were visualized and imaged using the EVOS M5000 Imaging System (ThermoFisher Scientific).

2.4 | AcidSensor tau labeling

Samples of the 2 μM protofibrillar stock were fluorescently tagged using the AcidSensor Labeling Kit (Dojindo A558), according to manufacturer's instructions. The NH_2-Reactive AcidSensor tag fluoresces at low pH conditions, allowing visualization of substances internalized by endocytosis. For this assay, hCMECs were seeded in 8-well chamber slides (Millipore) coated with attachment factor (Cell Systems 4Z0-201) and grown until confluence in EBM-2 supplemented with growth factors and 5% FBS. Cells were then treated with 25 nM pre-tagged protofibrillar tau for 1 hour in Hank's Balanced Salt Solution (HBSS; Gibco 14025092). After treatment, cells were washed with 1× phosphate-buffered saline (PBS), then fixed using 4% paraformaldehyde (PFA) in PBS (BeanTown Chemical) for 10 minutes at room temperature. Slides were imaged with a fluorescence-inverted deconvolution microscope (Nikon Eclipse Ti2) using the Cy5 filter (633 nm) and brightfield setting. Images were deconvolved with the 64-bit NIS Elements AR Analysis 5.360.02 image capturing and analysis software.

2.5 | Endothelial barrier resistance measurements

Cerebrovascular endothelial barrier formation was assessed using the Electrical Cell Impedance Sensing-Zθ (ECIS) system (Applied Biophysics). Barrier resistance experiments were performed in 8-well ECIS (8WE10+, Applied Biophysics; with 40 electrodes), or in 96-well (96W20idf Applied Biophysics; with 20 electrodes in an interdigitated configuration) gold-plated arrays pre-treated with 10 mM L-Cysteine (Alfa Aesar, A10435) for 15 minutes at room temperature then pre-coated with rat tail collagen (gibco, A10483-01), diluted 1:20 in 0.15 M NaCl according to the manufacturer's instructions. hCMECs (400,000 cells/ml) were seeded and monitored for ≈ 48 hours until the electrical resistance reached a plateau at a frequency of 4000 Hz. Upon reaching a resistance plateau indicative of barrier formation the cell monolayers were treated with 5 or 25 nM pre-aggregated 1n4r tau fibrils, 25 nM tau monomers, or the arachidonic acid-containing vehicle; all treatments were prepared EBM-2 media containing 1% FBS, which was used as control. Barrier permeability was then assessed for up to 48 hours post-treatment measured as a decrease in barrier resistance at 4000 Hz compared to control cells.

2.6 | Apoptotic cell death measurement

Presence of apoptotic cell death was assessed as formation of fragmented nucleosomes using the Cell Death Detection ELISA^{Plus} kit (Roche Applied Science) according to the manufacturer's instructions.[45] Briefly, 10,000 cells/well were seeded and, after 24 hours, treated with 5 or 25 nM pre-aggregated tau fibrils, in EBM-2 media supplemented with 1% FBS. Extranuclear DNA-histone complexes were measured with Cell Death Detection ELISA^{Plus} at 405 nm using the SpectraMax i3x Multi-Mode Microplate Reader (Molecular Devices). Results are expressed as percent change compared to control cells.

2.7 | Lactate dehydrogenase assay

Lactate dehydrogenase (LDH) release in the cell culture supernatant, indicative of necrosis, was assessed using the Cytotoxicity Detection Kit^{Plus} (Roche Applied Science) according to the manufacturer's instructions. The conversion of pyruvate to lactate by LDH results in the reduction of NAD^+ to NADH. The activity of LDH in the cell media was assessed as the production of red formazan from tetrazolium salt, an NADH-dependent reaction. Absorbance was measured at 490 nm using the SpectraMax i3x Multi-Mode Microplate Reader (Molecular Devices). Results are expressed as percent change compared to control cells.

2.8 | Caspase 3/7 fluorescence activity assay

hCMECs (10,000 cells/well) were seeded in 96-well tissue culture-treated plates and were treated with 5 nM tau, 25 nM tau or 300 μM H_2O_2 in 1% FBS/EBM-2 for 24 hours. At treatment endpoint, treatment media was replaced with 5 μM Caspase 3/7 Green Detection Reagent (Invitrogen, C10430) diluted in 1% FBS/EBM-2, which stains only cells with active caspase 3/7. Briefly, cells were incubated in the dye for 30 minutes at 37°C and 5% CO_2 and subsequently imaged (three randomized images/well) with a Brightfield and GFP filter using an EVOS M5000 imaging system. Images were analyzed by calculating the percentage of cleaved caspase positive cells to total number of cells, as described previously.[45]

2.9 | JP immunocytochemistry

Primary human cerebrovascular endothelial cells (hCECs) were seeded in 8-well chamber slides (Millipore) coated with attachment factor (Cell Systems 4Z0-201) and grown until 100% confluence in EBM-2 supplemented with growth factors and 5% FBS. Once a confluent monolayer was observed, the media was replaced to EBM-2 containing 0.25% FBS and bFGF (1:2000), for 2 to 3 days, with the last 3 to 24 hours being exposed to 25 nM pre-aggregated tau fibrils. After treatment, cells were fixed with 4% PFA (BeanTown Chemical) for 10 minutes at room temperature and blocked for 1 hour with 20 mg/mL bovine serum albumin (BSA; ThermoFisher Scientific). Cells were then incubated with ZO-1 (Invitrogen 61-7300, 1:100), phosphorylated VE-Cadherin (Tyr 658; Invitrogen 44-1144G, 1:100), VE-Cadherin (Invitrogen; 36-1900, 1:100), and HT7 (tau) primary antibodies (Invitrogen MN1000, 1:100) for 1.5 hours at room temperature in 5 mg/mL BSA + 0.01% triton-x100 (Sigma Aldrich T8787). After washes, cells were incubated with AlexaFluor 568 goat anti-rabbit (Life Technologies, A-11011) and AlexaFluor 647 goat anti-mouse (Life Technologies, A-21235) secondary antibodies for 1 hour (1:200 in PBS). Subsequently, slides were mounted with DAPI (blue) mounting media (Southern Biotech; 0100-20). Images were acquired with a fluorescence inverted microscope (Nikon Eclipse Ti2) and deconvolved with the 64-bit NIS Elements AR Analysis 5.360.02 image capturing and analysis software. Fluorescence intensity and line scan analysis was performed using Fiji (ImageJ).

2.10 | Western blotting

Assessment of protein expression was performed by western blot analysis using antibodies against VCAM-1 (abcam; ab134047, 1:1000), ICAM-1 (Invitrogen MA5407, 1:500), phosphorylated VE-Cadherin (Tyr 658; Invitrogen 44-1144G, 1:1000), VE-Cadherin (Invitrogen; 36-1900, 1:1000), superoxide dismutase 2 (SOD2; Cell Signaling Technologies, #13194S, 1:1000), matrix metalloproteinase 2 (MMP2; abcam 86607, 1:1000), and glucose transporter 1 (GLUT1; Novus Biological NB110-39113, 1:1000). Normalization was performed using anti-β actin (Millipore; MAB1501, 1:5000) or VDAC (Proteintech 66345-1-Ig, 1:5000). After gel electrophoresis on 4% to 12% Bolt Bis-Tris sodium dodecyl sulfate polyacrylamide gels, proteins were transferred to nitrocellulose membranes (0.45 μm pore size; Amersham, Cytiva Life Sciences) at 110 V for 70 minutes, using transfer buffer, containing 20% (v/v) methanol. Membranes were then blocked with 5% non-fat milk in Tris-buffered saline (TBS; or 5% BSA in TBS for phosphorylated proteins), and subsequently immunoreacted with the respective primary antibodies for each experiment, followed by incubation with the appropriate anti-rabbit or anti-mouse secondary antibodies (1:10,000; LICOR). Membranes were developed with the LICOR Odyssey CLx Immunoblot Imager and blots were analyzed using the LICOR Image Studio software.

2.11 | Glycolysis and mitochondrial stress test

Glycolysis and mitochondrial respiration rates were measured through extracellular acidification rate (ECAR) and oxygen consumption rate (OCR) in hCMECs using the Seahorse XFe96 or XF Pro Analyzer (Agilent Technologies). Cells were seeded in a density of 2.0×10^4 cells/well and treated as described previously for 3, 24, 48, or 72 hours. We performed a glycolysis stress test (GST) or mitochondrial stress test (MST) according to manufacturer's recommendations. Briefly, for GST, treatment medium was replaced with XF Assay Medium supplemented with 2 mM L-glutamine. Prior to assay, cells were pre-equilibrated in the assay medium by in a 37°C incubator without CO2 for 45 min. Non-glycolytic ECAR measurements were performed; then, subsequent ECAR measurements were performed after injection of 10 mM glucose, 1.5 μM oligomycin, and 50 mM 2-deoxy-glucose. For MST, the procedure was performed as described above, with the XF assay medium supplemented with 1 mM pyruvate, 10 mM glucose, and 2 mM L-glutamine. After basal OCR measurements, subsequent OCR measurements were performed after injection of 1.5 μM oligomycin, 1 μM carbonyl cyanide 4-(trifluoromethoxy) phenylhydrazone (FCCP) and 0.5 μM rotenone + 0.5 μM antimycin A. Results were extracted using the Wave report generator and normalized to total protein

concentration per well, assayed by Pierce 660 nm Protein Assay Reagent (ThermoFisher Scientific).

2.12 | Cytokine production assays

Production and release of pro-inflammatory cytokines was assessed using a V-Plex Proinflammatory Panel 1 (Human) kit from Meso Scale Discovery (MSD), which measures the expression of 10 cytokines per sample. hCMECs (350,000 cells/well) were seeded in 6-well plates and treated as previously described for 3 and 24 hour time points. After treatment, conditioned media was stored at −80°C until the assay was conducted. The procedure was carried out according to manufacturer's recommendations and cytokine concentration was normalized to total protein concentration in each sample, assayed by Pierce BCA Protein Assay Kit (ThermoFisher Scientific).

2.13 | Cell viability assay

EC viability challenged with heptelidic acid (HA), a known GAPDH inhibitor, was determined by WST-1 colorimetric assay (Millipore Sigma, 5015944001), which is based on tetrazolium salt cleavage by mitochondrial dehydrogenases in which an increase in formazan dye formation represents the number of viable cells, due to increased activity of these enzymes. Briefly, hCMECs (10,000 cells/well) were seeded in 96-well cell culture plates. The next day, cells were treated with increasing concentrations of HA ranging from 50 to 1000 nM (in triplicate) in a total volume of 100 µL per well for 24 hours. After treatment, 10 µL of ready-to-use WST-1 dye was added to each well, cells were then incubated for 4 hours at 37°C. After incubation with the day, absorbance was read at 450 nm using the SpectraMax i3x Multi-Mode Microplate Reader (Molecular Devices). Results are expressed as percent change compared to control cells.

2.14 | Immunocytochemistry for tau and β-III tubulin

hCMEC cells were seeded in 8-well chamber slides (Millipore) coated with attachment factor (Cell Systems 4Z0-201) and grown until confluence in EBM-2 supplemented with growth factors and 5% FBS. Cells were then treated with 25 nM pre-aggregated tau fibrils or human tau fibrils (diluted to 25 nM) for 24 hours. After treatment, cells were fixed with 4% PFA (BeanTown Chemical) for 10 minutes at room temperature, permeabilized using 0.1% Triton X-100 for 10 minutes, and blocked for 1 hour in 3% BSA. Cells were then incubated with HT7 (Invitrogen MN1000, 1:00) and β-III tubulin (Invitrogen PA5-81099, 1:300) at 1.5 hours at room temperature in 1% BSA. After washes, cells were incubated with AlexaFluor 568 goat anti-rabbit and Alexa Fluor488 goat anti-mouse (Life Technologies, A-11001) secondary antibody for 1 hour (1:200 in PBS). Subsequently, slides were mounted with DAPI (blue) mounting media (Southern Biotech; 0100-20). Images were acquired with a fluorescence inverted microscope (Nikon Eclipse Ti2) and deconvolved with the 64-bit NIS Elements AR Analysis 5.360.02 image capturing and analysis software. Fluorescence intensity was analyzed by Fiji (ImageJ).

2.15 | Mitochondrial membrane potential imaging

hCMECs (50,000 cells/well) cells were seeded in 8-well chamber slides and grown as previously described. Cells were then treated with 5 or 25 nM protofibrillar tau for 48 hours in EBM-2 supplemented with 1% FBS. After treatment, cells were washed with HBSS and incubated with MitoTracker Red CM-H2Xros (Invitrogen, M7513), which stains only mitochondria with a healthy membrane potential, diluted to a final concentration of 250 nM in HBSS for 30 minutes at 37°C. Slides then washed with HBSS, fixed using 4% PFA (BeanTown Chemical) for 10 minutes at room temperature and mounted onto coverslips with DAPI (blue) mounting media. Slides were then imaged with a fluorescence inverted microscope (Nikon Eclipse Ti2). Images were deconvolved with the 64-bit NIS Elements AR Analysis 5.360.02 image capturing and analysis software.

2.16 | P301S (PS19) mouse model

Male and female P301S mice, a widely used model of tauopathy, and age-matched wild-type (WT) littermates were bred internally. Mice were maintained under controlled conditions (≈ 22°C, under a 12 hour light–dark cycle, lights on 7 am to 7 pm) with unrestricted access to food and water. The generation of P301S (PS19) mice was as initially described in Yoshiyama et al.[46] PS19 mice start developing age-dependent decrease in tau solubility between 3 and 6 months of age, synaptic pathology starting at 3 months, with no apparent neuronal loss, PHF-1 (phospho-Ser396- and phospho-Ser404-tau) positivity or NFT formation up to 6 months of age. Weak astrogliosis throughout the brain, and microglial activation mainly in the hippocampal region, were present in 3- to 4-month-old PS19 mice.[46] Mice were sacrificed at 3 months of age, before NFT formation and neuronal loss, for cerebral vessel extraction, as well as tissue extraction for biochemical and/or immunohistochemical analysis. All experiments and animal protocols were performed according to protocols approved by the Institutional Animal Care and Use Committee of Temple University School of Medicine and conformed to the National Research Council Guide for the Care and Use of Laboratory Animals published by the US National Institutes of Health (2011, eighth edition).

2.17 | Cerebral vessels isolation

The cerebral microvasculature of 3-month-old WT and PS19 mice was performed as described in Lee et al.[47] with modifications. Briefly, mice were euthanized and underwent transcardiac perfusion with ice-cold PBS. Afterward, mice brains were dissected, separating cerebellum and

olfactory bulb. Mechanical dissociation of the brain hemispheres in MCDB131 medium (gibco, 10372019) was performed using a Teflon potter homogenizer and tissue homogenate was centrifuged (4°C) for 5 minutes at 2000 × g. The myelin-containing pellet was then resuspended in 17.5% dextran (Sigma Aldrich 31390) and centrifuged (4°C) for 15 minutes at 10,000 × g; subsequently, the pellet (microvessels) was resuspended in ice-cold PBS and washed through using a 40 μm cell straining (Corning), before processing as described below.

2.18 | Vessel immunocytochemistry

After vessel wash-through, vessels were submerged in 4% PFA in a shaker for 15 minutes at room temperature. Vessels were washed through again with PBS and retrieved using 1% BSA by reverse filtering, then centrifuged (4°C) for 10 minutes at 2000 × g. The pellet was then resuspended in 200 μL PBS and ≈ 30 μL drops were placed on Superfrost Plus microscope slides (ThermoFisher Scientific, 1255015). Slides were then blocked for 1 hour in 5% BSA and then incubated with ZO-1 (Invitrogen 61-7300, 1:100), Claudin-5 (invitrogen 35-2500, 1:100), CD-31 (BD Biosciences 550274, 1:50), α-SMA (abcam ab5694, 1:250), and HT7 primary antibodies (Invitrogen MN1000, 1:100) in 5% BSA + 0.1% Triton X-100 overnight (4°C). The next day, slides were washed and incubated with AlexaFluor 568 goat anti-rabbit (Life Technologies, A-11011), AlexaFluor 488 goat anti-mouse (Life Technologies, A-28175), and AlexaFluor 647 goat anti-rat (Life Technologies, A-21247) secondary antibodies for 1 hour (1:200 in PBS). Subsequently, slides were mounted with DAPI (blue) mounting media (Southern Biotech; 0100-20). Images were acquired with a fluorescence inverted microscope (Nikon Eclipse Ti2) and deconvolved with the 64-bit NIS Elements AR Analysis 5.360.02 image capturing and analysis software. Fluorescence intensity and colocalization was analyzed by Fiji (ImageJ).

2.19 | Vessel mitochondrial stress test

We performed Extracellular Flux Analysis (MST) on isolated cerebral microvessels as described in Sure et al.[48] After vessel wash-through, vessels were retrieved using 0.5% BSA-MCDB 131 by reverse filtering, then centrifuged (4°C) for 10 minutes at 5000 × g. The pellet was then resuspended in 600 μL XF assay medium (supplemented with 1 mM pyruvate, 10 mM glucose, and 2 mM L-glutamine). 50 μL vessels were plated onto Seahorse XF 96-well microplates and centrifuged (room temperature) for 10 minutes at 1500 × g. Afterward, vessels were brought to total volume (180 μL) and were pre-equilibrated in the assay medium in a 37°C incubator without CO_2 for 30 minutes. After basal OCR measurements, subsequent measurements were performed after injection of 2.5 μM oligomycin, 1.5 μM FCCP, and 10 μM rotenone + 10 μM antimycin A. For ATP Production Rate assay, subsequent measurements were performed after injection of 2.5 μM oligomycin and 10 μM rotenone + 10 μM antimycin A. Results were extracted using the Wave report generator and normalized to total protein concentration per well, assayed by Pierce 660 nm Protein Assay Reagent (ThermoFisher Scientific).

2.20 | Vessel cytokine production

After vessel wash-through, vessels were retrieved using 0.5% BSA-MCDB 131 by reverse filtering and incubated for 3 hours in a humidified cell culture incubator under a 5% CO_2 atmosphere at 37°C. Media was aliquoted for further analysis and vessels were lysed in 100 μL cold tissue homogenization buffer (250 mM sucrose, 20 mM Tris Base pH 7.4, 1 mM EDTA, 1 mM EGTA + phosphatase/protease inhibitors). The pellet was sonicated for 30 seconds at 50 amplitudes on ice and centrifuged for 10 minutes at 10,000 × g for 4°C. Supernatant was aliquoted, protein concentration was determined by Pierce 660 nm Protein Assay Reagent, and equal volumes were loaded in duplicate in the V-Plex Proinflammatory Panel 1 (mouse) MSD plate. The assay was conducted according to manufacturer's recommendations.

2.21 | Statistical analysis

All experimental graphs are representative of at least three independent experiments with two or more technical replicates. For each Seahorse experiment performed with hCMECs, we assayed a minimum of eight replicates per condition. Data are represented as mean ± standard error of the mean. Prior to statistical analysis, outliers were identified and removed using the ROUT method on GraphPad software. Statistical significance was assessed by Student *t* test, one-way analysis of variance (ANOVA), or two-way ANOVA followed by a Tukey post hoc test using GraphPad Prism 10. Statistically significant differences required a P value ≤0.05.

3 | RESULTS

3.1 | Protofibrillar tau impairs endothelial barrier resistance, independently of cell death

The presence of tau aggregates on and within the vascular wall has been described in both human and mouse tauopathy models.[13,14] Oligomeric and protofibrillar tau aggregates can reach the ECs that line the lumen of cerebral blood vessels through tau spreading via astrocytic end feet or neuronal processes or through brain perivascular clearance processes.[49,50] Although both oligomeric and protofibrillar tau aggregates have been shown to induce cytotoxicity in neuronal and glial cells, the toxic effects of tau protofibrils or fibrils on cerebral ECs and the BBB remain understudied.

Here, we first sought to determine whether tau protofibrillar species have a detrimental effect on cerebral EC barrier resistance. To study this, we aggregated monomeric 1N4R tau into protofibrillar species using arachidonic acid as a fibrillization inducer, according to published protocols.[41] We confirmed the degree of aggregation by TEM after negative staining with 1% uranyl acetate as a fixative (Figure 1A, scale bar 600 nm), which revealed the formation of primarily fibrillar species of ≈ 200 nm in length, which are typically classified as protofibrils.[51,52] To confirm that these protofibrillar species enter

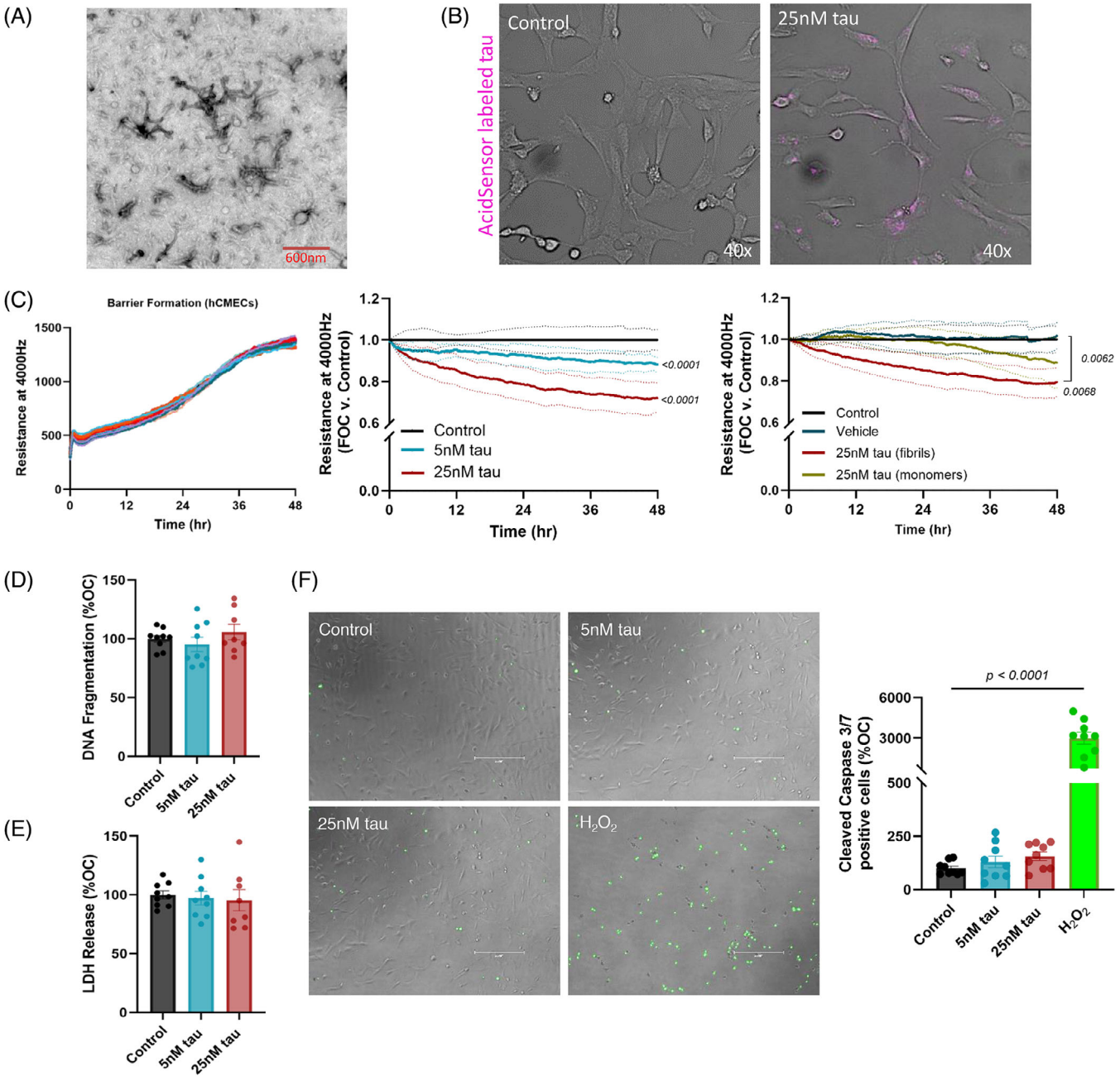

FIGURE 1 Protofibrillar tau induces loss of barrier resistance independently of cell death. A, Transmission electron microscope analysis of tau aggregates after negative staining with 1% uranyl acetate, reveals primarily protofibrillar species (scale bars 600 nm). B, One hour of treatment with AcidSensor-labeled protofibrillar tau demonstrates early internalization in hCMECs. C, Left panel TEER (at 4000 Hz) measurement of hCMECs with the ECIS Zθ system illustrates barrier formation at about 48 hours after plating. Middle panel: TEER of hCMECs monolayers treated with 5 or 25 nM fibrillar tau, measured over time for 48 hours, indicates progressive loss of barrier resistance induced by protofibrillar tau species. Right panel: TEER of hCMECs treated with fibrillization vehicle, protofibrillar or monomeric tau (25 nM) for 48 hours (right). Data are represented as change in resistance normalized to the untreated control, $n = 3$ experiments with two replicates per condition. D, Apoptosis, measured as DNA fragmentation, of hCMECs treated for 24 hours with 5 or 25 nM tau. E, LDH release for hCMECs treated for 24 hours with 5 or 25 nM tau. F, Caspase 3/7 fluorescence in hCMECs treated with aggregated tau for 24 hours, or H_2O_2 as a positive control (left), with quantification of caspase positive cells (right). **Statistical significance established by one-way ANOVA (Cell Death ELISA, LDH); Tukey post test. Two-way ANOVA (ECIS). Significant *P* values are reported in the graphs. ANOVA, analysis of variance; hCMEC, human cerebral microvascular endothelial cell; LDH, lactate dehydrogenase; TEER, trans-endothelial electrical resistance.

ECs, we fluorescently tagged our tau stock with an NH2-reactive pH-dependent probe (Dojindo) that emits fluorescence when the protein is in acidic conditions, such as in late endosomes/lysosomes. As early as 1 hour after treatment of hCMECs with 25 nM protofibrillar tau, we observed fluorescence within the cell body (Figure 1B), indicating tau entry in intracellular acidic compartments. We then tested the effects of these protofibrillar tau species on the endothelial barrier, using the ECIS ZΘ system (Applied Biophysics) to monitor trans-endothelial electrical resistance (TEER) over time. The endothelial monolayer displayed barrier formation, measured by TEER at 4000 Hz, at ≈ 48 hours after seeding (Figure 1C, left). After a steady plateau in the TEER trace, we treated the EC monolayer with 5 or 25 nM protofibrillar tau. Both concentrations of tau induced a dose-dependent decrease in barrier resistance, corresponding to an increase in barrier permeability, compared to control cells (Figure 1C, middle). We then compared the effects of pre-aggregated tau protofibrils to those of monomeric tau. We observed that monomeric tau starts inducing a decrease in barrier resistance after 24 hours of incubation with the EC monolayer, while protofibrillar aggregates induce an immediate and steady reduction in TEER, suggesting that aggregation of tau (such as that occurring in the cell media after treatment, or pre-aggregation into protofibrils) is necessary for the observed effects on BBB permeability. As a control, we also treated the EC barrier with the fibrillization vehicle alone, which had no effects on TEER, confirming that the effects induced by protofibrillar tau are primarily due to the tau aggregates themselves and not to other substances present in the aggregation vehicle (Figure 1C, right).

Tau intermediate aggregates such as oligomers or protofibrils have been characterized as cytotoxic to several cell types, including neurons; therefore, to exclude that the effects on barrier resistance were due to tau cytotoxicity, we assessed EC death (both apoptosis and necrosis) at 24 hours, a time point when a steady decline in barrier resistance was evident (Figure 1C, middle). We measured DNA fragmentation, a late event in the apoptotic pathway, using a Cell Death ELISA^{PLUS} kit (Roche), and observed no changes upon tau treatment (Figure 1D). LDH release into the cell supernatant (Figure 1E), indicative of necrosis, also showed no changes, confirming that the effects on loss of barrier resistance are independent of tau-induced cell death. Further, we tested caspase 3/7 activation using a Caspase 3/7 CellEvent assay, after 24 hours of treatment with 5 or 25 nM protofibrillar tau, using H_2O_2 as a positive control; we observed no significant changes in caspase activation, confirming the absence of apoptotic cell death (Figure 1F).

3.2 | Protofibrillar tau causes loss of JP expression and integrity

To further understand the mechanisms responsible for the observed loss of TEER, we assessed changes in the tight-JPs that line the cerebral EC membrane. For this purpose, we used primary human cerebral endothelial cells (hCECs), as these cells exhibit greater contact inhibition and form stronger tight junctions in control conditions. Immunocytochemical assessment of zonula occludens 1 (ZO-1) and VE-Cadherin after 24 hours of treatment with protofibrillar tau revealed more breaks along the lining of the cell (Figure 2A,B). Quantification of fluorescence intensity revealed a decrease in the expression of ZO-1 and VE-Cadherin for the cells treated with protofibrillar tau, compared to control (Figure 2C). Staining with HT7 anti-tau antibody confirmed entry of protofibrillar tau within ECs. Line scan analysis highlights the discontinuity in VE-Cadherin and ZO-1 (Figure 2D,E) fluorescence along the cell membrane, indicating a loss of junction integrity due to the presence of aggregated tau. Interestingly, we observed localization of tau both intracellularly and lining the cell membrane, suggesting that the effects of tau on BBB and JPs could be mediated by both membrane-binding and/or intracellular mechanisms.

3.3 | Tau protofibrils induce EC metabolic alterations associated with pro-inflammatory EC activation

While peripheral ECs have been characterized as primarily glycolytic,[29,31] brain ECs have an increased need for mitochondrial ATP production.[53] Furthermore, increased glycolysis in ECs has been linked to a switch toward an inflammatory phenotype,[26,37] and maintenance of the endothelial barrier is an energy-taxing process.[26,35,54] Due to this relationship, we decided to examine whether protofibrillar tau aggregates induced alterations in endothelial bioenergetic processes and inflammatory activation. We measured endothelial glycolysis by extracellular flux using a Seahorse XF96 Analyzer. A GST (Figure 3A) on hCMECs treated with protofibrillar tau for 24 hours indicated an increase in glycolysis and glycolytic capacity parameters, measured by ECARs and normalized to protein concentration (Figures 3B and S1A in supporting information). Further, we assessed mitochondrial respiration (OXPHOS) through a Seahorse Mitochondria Stress Test and observed no changes in OCRs at 24 hours (Figure S1B,C). We then questioned whether this increase in glycolytic metabolism represented a sustained response starting at earlier time points. Thus, we assessed a 3 hour time point as an acute response to tau challenge and we observed increased glycolytic rates with both concentrations of tau (Figure 3C,D), suggesting that this is likely a response to the aggregated tau treatment.

Because of the known association between increased glycolysis and EC inflammatory activation, we tested whether adhesion molecules that localize toward the vessel lumen and mediate leukocyte rolling during inflammatory events are modulated at these time points. We observed a significantly increased expression of VCAM-1 after challenge with protofibrillar tau at 24 hours (Figure 3E), but no changes in the expression of ICAM-1. We observed a broader activation of ECs at 3 hours, with increased expression of both VCAM-1 (with both concentrations of tau) and ICAM-1 (significant with 25nM tau; Figure 3F). Cytokine production may be one of the earliest events mediating neuroinflammation and BBB permeability. Thus, to understand if these endothelial pro-inflammatory phenotypes are due to changes in cytokine production and release into the cell supernatant, we performed a MSD multiplex cytokine assay, in which we observed

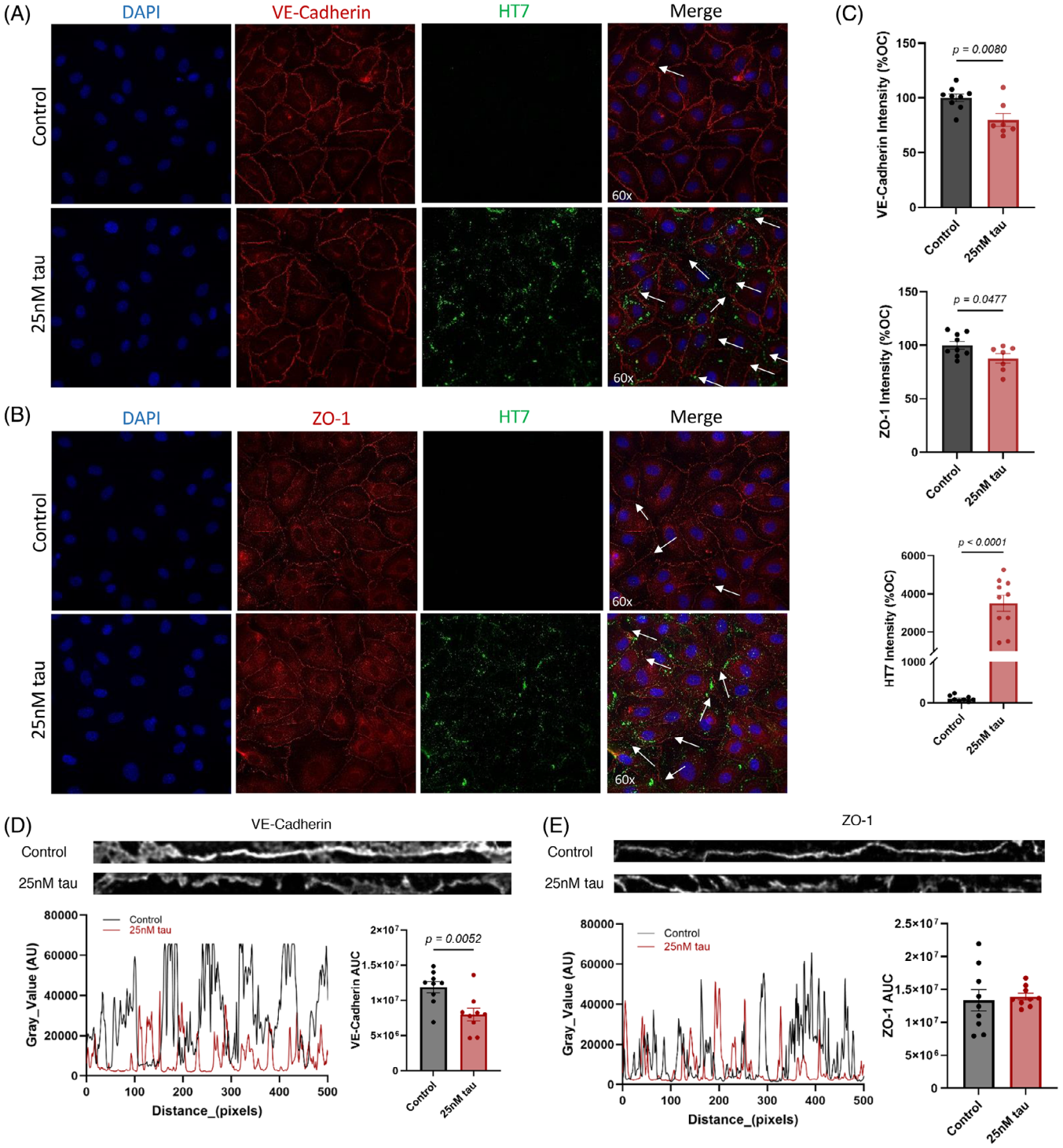

FIGURE 2 Loss of junction protein integrity mediated by protofibrillar tau. A–B, Immunocytochemical assessment of junction proteins ZO-1 (A) and VE-Cadherin (B) (red) on hCECs 24 hours post treatment with protofibrillar tau (green). Arrows indicate breaks on junctions staining. C, Quantification of fluorescence intensity for ZO-1 (top), VE-Cadherin (middle), and tau (bottom), expressed as percent of change compared to control (%OC). D, Representative line scan of VE-Cadherin intensity across the barrier staining, with accompanying intensity graph below. E, Representative line scan of ZO-1 intensity across the barrier staining, with accompanying intensity graph below. Statistical significance established by Student *t* test. Significant *P* values are reported in the graphs. hCECs, primary human cerebral endothelail cells.

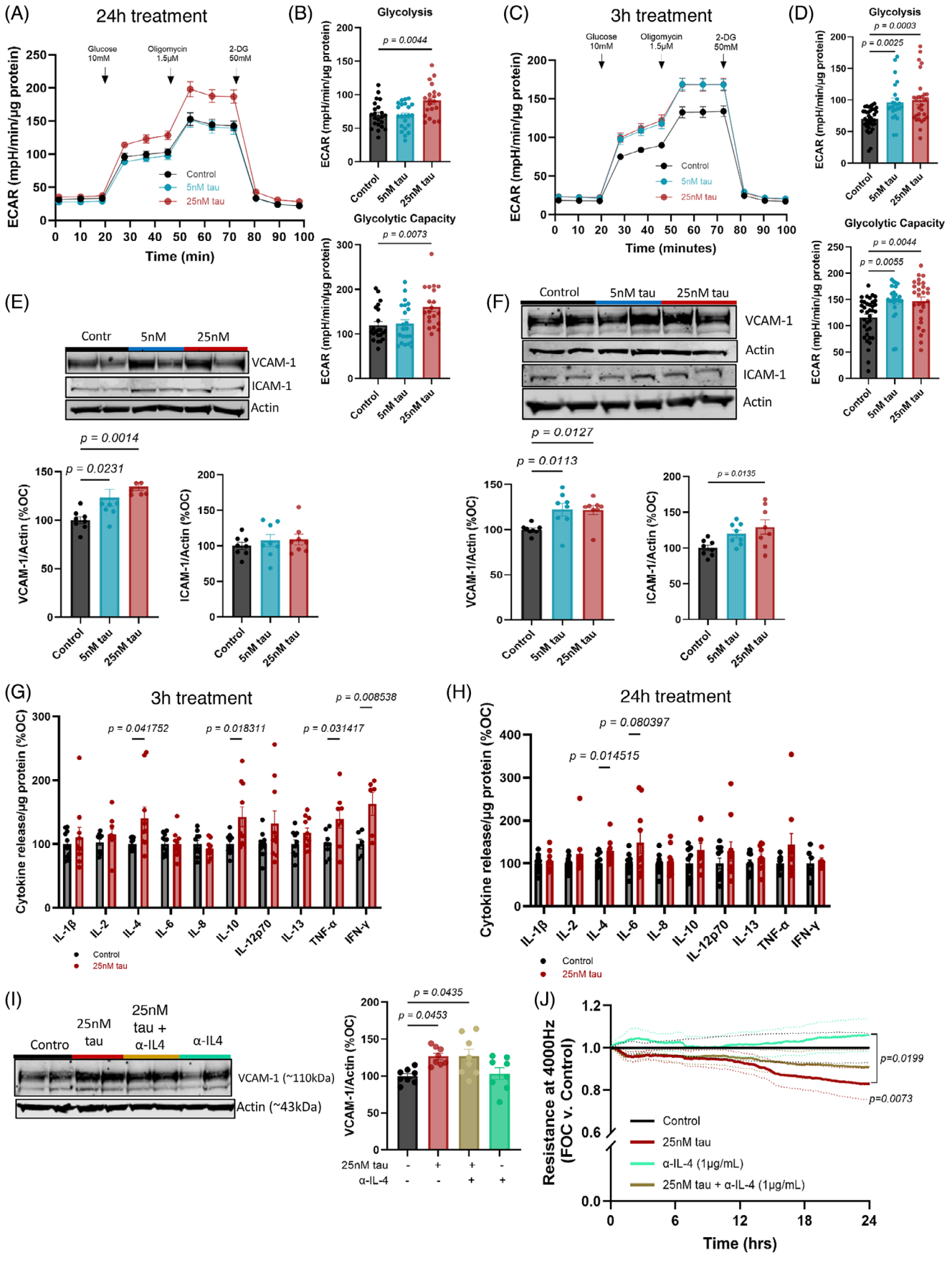
(A)
24h treatment
Glucose 10mM
Oligomycin 1.5µM
2-DG 50mM
ECAR (mpH/min/µg protein)
Time (min)
Control
5nM tau
25nM tau
(B)
Glycolysis
p = 0.0044
Glycolytic Capacity
p = 0.0073
(C)
3h treatment
Time (minutes)
(D)
Glycolysis
p = 0.0003
p = 0.0025
Glycolytic Capacity
p = 0.0044
p = 0.0055
(E)
Contr
5nM
25nM
VCAM-1
ICAM-1
Actin
p = 0.0014
p = 0.0231
VCAM-1/Actin (%OC)
ICAM-1/Actin (%OC)
(F)
p = 0.0127
p = 0.0113
p = 0.0135
(G)
3h treatment
p = 0.008538
p = 0.041752
p = 0.018311
p = 0.031417
Cytokine release/µg protein (%OC)
IL-1β
IL-2
IL-4
IL-6
IL-8
IL-10
IL-12p70
IL-13
TNF-α
IFN-γ
(H)
24h treatment
p = 0.080397
p = 0.014515
(I)
Contro
25nM tau
25nM tau + α-IL4
α-IL4
VCAM-1 (~110kDa)
Actin (~43kDa)
p = 0.0435
p = 0.0453
25nM tau
α-IL-4
(J)
Resistance at 4000Hz (FOC v. Control)
p=0.0199
p=0.0073
α-IL-4 (1µg/mL)
25nM tau + α-IL-4 (1µg/mL)
Time (hrs)

an increase in interleukin (IL)-4, interferon gamma (IFN-γ), and tumor necrosis factor alpha (TNF-α) production and release after 3 hours of 25nM protofibrillar tau challenge (Figure 3G). Interestingly, anti-inflammatory cytokine IL-10 was also increased at 3 hours, suggesting an early compensatory response, which was reversed at 24 hours. IL-4 production and release was sustained after 24 hours of tau treatment, with increasing trends in IL-6 production, suggesting a continuous inflammatory response (Figure 3H). Additionally, immunocytochemical analysis indicated an increase in the phosphorylated form of VE-Cadherin, which is known to be internalized in hCECs and subsequently degraded, losing its functionality, 3 hours post-treatment (Figure S2 in supporting information). Because IL-4 has previously been shown to induce hyperpermeability of coronary arterial ECs,[55] and IL-4 upregulation was evident at both 3 and 24 hours after tau challenge, we decided to evaluate the potential of IL-4 as a mediator of the loss of endothelial barrier resistance. To test this hypothesis, we used a neutralizing antibody against IL-4. However, treatment with tau in the presence of the IL-4 antibody did not prevent the increase in VCAM-1 induced by 25 nM protofibrillar tau (Figure 3I) and resulted only in a partial recovery of TEER decline (Figure 3J). Overall, these data indicate an early activation of glycolysis correlating with an endothelial inflammatory phenotype and BBB dysfunction, starting acutely after protofibrillar tau stimulation.

3.4 | Inhibition of glycolysis maintains barrier function and suppresses tau-mediated endothelial activation

We hypothesized that that tau-mediated metabolic alterations may be causal to pro-inflammatory EC activation and loss of BBB resistance. Hence, we treated cells with both aggregated tau and a non-lethal concentration (100 nM) of HA[56] (cell viability in Figure S3A in supporting information), a potent GAPDH inhibitor, to reverse the increase in glycolysis. Co-treatment with HA decreased tau-mediated IL-4 production at 24 hours (Figure 4A) and reduced tau-induced VCAM-1 overexpression, as determined by western blot analysis (Figure 4B). Further, HA treatment completely prevented tau-mediated loss of barrier function (Figure 4C). We then questioned if the observed tau-mediated increase in glycolysis was dependent on inhibition of the first step of the glycolytic pathway. To this end, we used 2-deoxyglucose (2-DG), a competitive inhibitor for hexokinase, at non-lethal concentrations (cell viability in Figure S3B). Although treatment with 2-DG alone at baseline, as expected due to ECs being primarily glycolytic, decreases barrier resistance (Figure S3C), limiting glycolysis by 2-DG treatment 3 hours after tau insult, when glycolytic metabolism is increased (as reported above and in Figure 3C,D), significantly and substantially rescued barrier function (Figure 4D). Overall, these results suggest that the overactivation of glycolytic processes is necessary for the pro-inflammatory EC activation and loss of barrier function induced by protofibrillar tau.

3.5 | Endothelial metabolic impairment and cell death are initiated after chronic protofibrillar tau treatment

To better understand whether chronic treatment with protofibrillar tau eventually results in EC cytotoxicity and death, we treated ECs with tau for longer time points. After 48 hours of challenge, we observed that apoptotic cell death, measured as DNA fragmentation (Figure 5A), was significantly increased by 25 nM tau (and trended to increase with 5 nM tau; $P = 0.0528$), with no secondary necrosis (Figure S4A in supporting information). At the same time point, the expression of VCAM-1 was decreased by 25 nM tau (Figure 5B), reverting from the upregulation observed earlier, and in line with the cytotoxicity at this time point. Moreover, the previous increase in glycolysis was not observed after 48 hours of tau challenge (Figures 5C and S4B). On the other hand, we observed an increase in mitochondrial OXPHOS, particularly basal and maximal respiration rates, as well as mitochondrial ATP production (Figure 5D,E) with 5 nM tau, but not 25 nM, which may be linked to a compensatory increase in energy production at the initial phases of pro-apoptotic pathways with the lower tau concentration.[57,58] To further characterize this effect, we assessed mitochondrial reactive oxygen species (mtROS)-mediated mechanisms and mitochondrial membrane potential. As shown in Figure 5F, we

FIGURE 3 Metabolic alterations induced by protofibrillar tau in association with pro-inflammatory endothelial cell activation. A, Representative trace for glycolysis stress test ECAR measurement using a Seahorse XF96 extracellular flux analyzer in hCMECs treated with aggregated tau for 24 hours. B, ECAR analysis indicates increased glycolysis (top) and glycolytic capacity (bottom) in the presence of 5 or 25 nM tau for 24 hours. C, Representative ECAR trace for glycolysis stress test in hCMECs treated with aggregated tau for 3 hours. D, ECAR indicates increased glycolysis (top) and glycolytic capacity (bottom) after 3 hours of protofibrillar tau challenge. E, Expression of adhesion markers VCAM-1 and ICAM-1 at 24 hours post treatment with 5 and 25 nM tau, as determined by western blot analysis. F, Expression of adhesion markers VCAM-1 and ICAM-1 at 3 hours post treatment with 5 and 25 nM tau. G, Increased IL-4, IL-10, TNF-α, and IFN-γ release after 25 nM tau treatment for 3 hours, determined by MSD proinflammatory panel analysis. H, Increased levels of IL-4 and increasing trends of IL-6 released in the media of hCMECs treated with 25 nM protofibrillar tau for 24 hours. I, Treatment with α-IL-4 does not decrease VCAM-1 expression in hCMECs at 24 hours post-tau treatment. J, TEER measurements during co-treatment with tau protofibrils (25 nM) and a neutralizing antibody against IL-4 (α-IL-4) only demonstrate a partial recovery against tau-mediated loss of barrier resistance. Statistical significance established by one-way analysis of variance; (WB), Seahorse (SH), and Tukey post hoc test, multiple unpaired *t* test (MSD). Significant *P* values are reported in the graphs. ECAR, extracellular acidification rate; hCMEC, human cerebral microvascular endothelial cell; ICAM-1, intercellular adhesion molecule 1; IFN-γ, interferon gamma; IL, interleukin; MSD, Meso Scale Discovery; TEER, trans-endothelial electrical resistance; TNF-α, tumor necrosis factor alpha; VCAM-1, vascular cell adhesion molecule 1; WB, western blot.

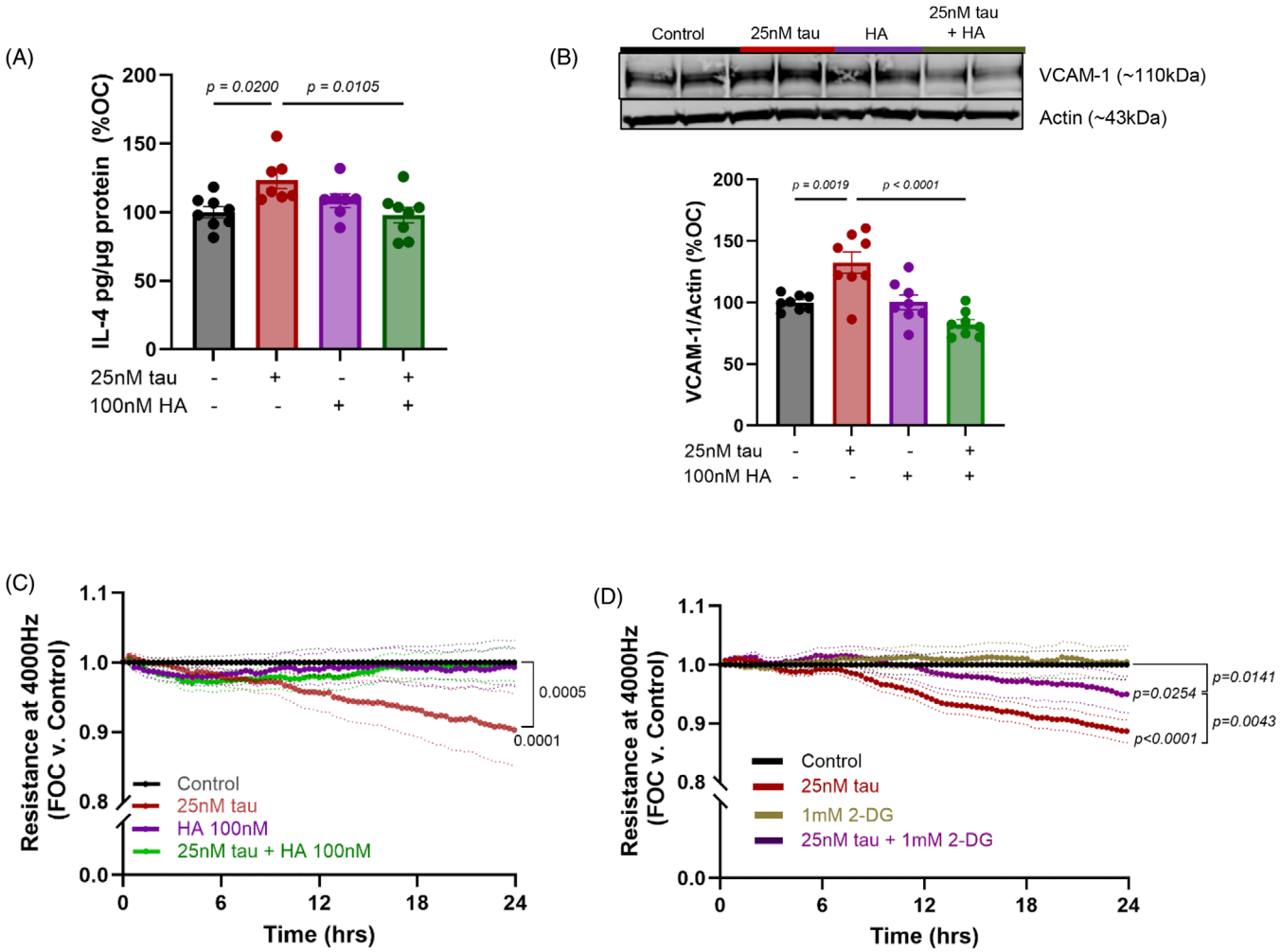

FIGURE 4 Modulation of glycolytic metabolism reverts fibrillar tau-mediated loss of barrier resistance. A, HA decreases tau-mediated IL-4 production in hCMECs 24 hours after treatment. B, Western blot analysis of hCMECs co-treated with tau and HA reveals a decrease in VCAM-1 expression in the presence of the glycolysis inhibitor. C, TEER measurement after co-treatment with protofibrillar tau and 100 nM HA indicates that blocking glycolysis prevents tau-mediated loss of barrier resistance. D, 2-deoxyglucose partially rescues tau-mediated loss of barrier resistance after 3 hours of tau treatment. Statistical significance established by one-way ANOVA (WB), and Tukey post hoc test, two-way ANOVA (Electrical Cell Impedance Sensing-Zθ). Significant *P* values are reported in the graphs. ANOVA, analysis of variance; hCMEC, human cerebral microvascular endothelial cell; HA, heptelidic acid; IL, interleukin; TEER, trans-endothelial electrical resistance; VCAM-1, vascular cell adhesion molecule 1; WB, western blot

observed an increase in membrane potential through analysis with MitoTracker Red CMX-H_2ROS dye (which enters mitochondria only upon a healthy membrane potential), correlating with increased respiration rates and ATP production observed after challenge with 5 nM tau. Accordingly, we observed an increase in the expression of mitochondrial SOD2, which is known to become upregulated to counteract excessive mtROS,[59] with the lower tau concentration (Figure 5G). These results suggest a possible compensatory mechanism by which, after long exposure to lower concentrations of aggregated tau species, ECs can over-activate OXPHOS and upregulate SOD2, in an attempt to overcome apoptosis, while at higher concentrations of aggregated tau these protective mechanisms fail to be activated.

Indeed, after 72 hours of treatment, the cytotoxic effects induced by 25 nM protofibrillar tau were even more evident, as determined by increased DNA fragmentation (Figure 5H) and LDH release (Figure 5I), suggesting secondary necrosis, while in the presence of 5 nM tau, both apoptosis and necrosis levels were similar to control cells. However, metabolic dysregulation was evident at 72 hours for both concentrations of tau, as indicated by reduced basal respiration (Figures 5J and S4C) and decreased glycolytic rates (Figures 5K and S4C), indicating that, at this time point, both concentrations of protofibrillar tau start stimulating toxic mechanisms, which are at a more advanced stage with higher tau concentrations.

3.6 | Human-derived tau fibrils decrease barrier function and induce pro-inflammatory EC phenotype

To confirm our results with more physiological fibrillar tau species, we challenged ECs with 25 nM fibrillar tau obtained from human AD

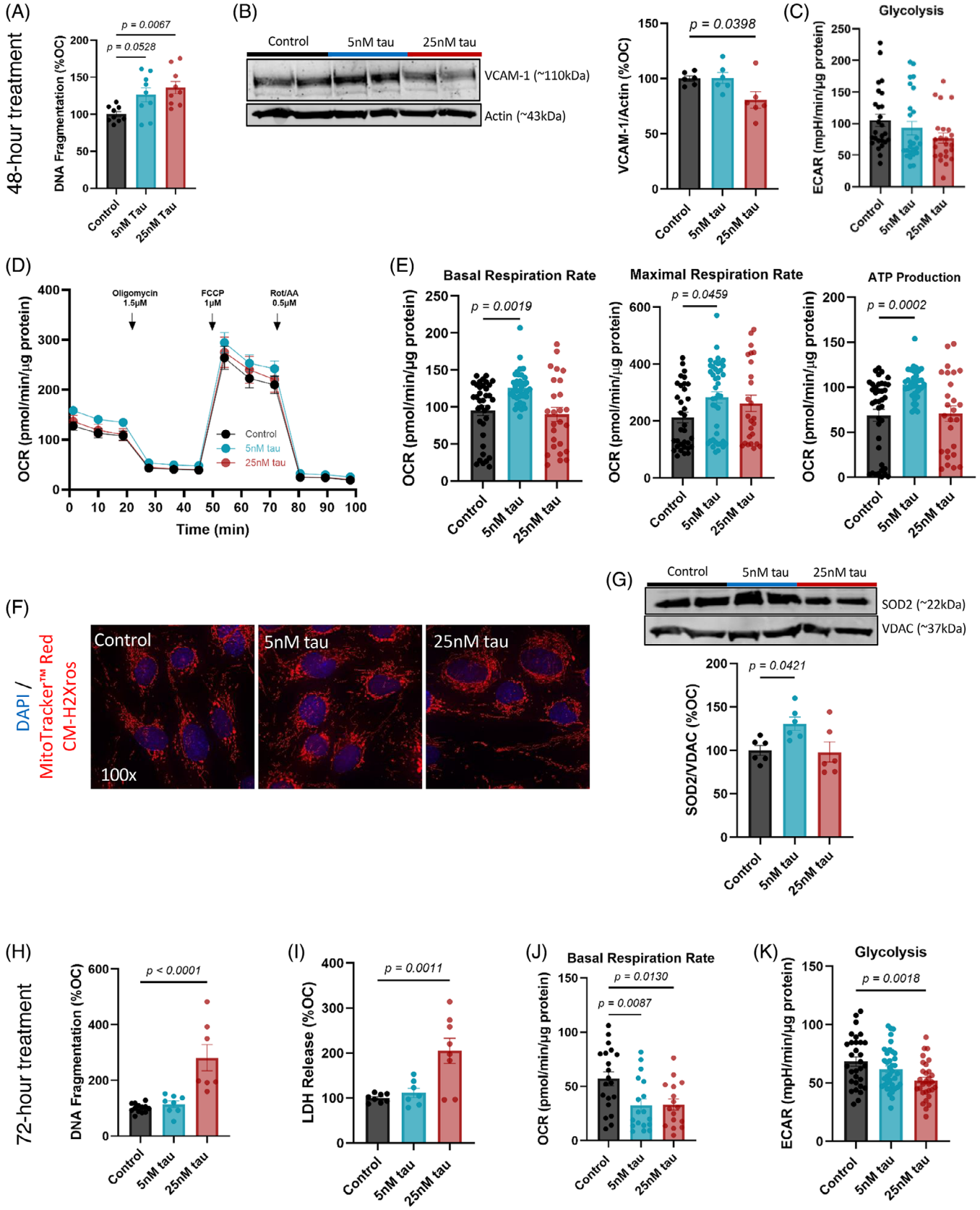

FIGURE 5 Mitochondrial OXPHOS alterations and endothelial cell death after longer treatment with protofibrillar tau. A, DNA fragmentation in hCMECs is increased 48 hours post-treatment with protofibrillar tau. B, Adhesion molecule VCAM-1 is decreased 48 hours post-treatment with 25 nM tau but not 5 nM tau, as determined by western blot analysis. C, Extracellular acidification rate demonstrate no changes in glycolytic rates at 48 hours. D, Representative trace for OCR (mitochondrial stress test) measured using a Seahorse XF96 Extracellular flux Analyzer. E, OCR

brain extracts (a generous gift from Dr. Rakez Kayed, UTMB).[42] Indeed, we observed a similar decrease in barrier resistance when the human fibrils were compared to our aggregated synthetic tau (Figure 6A). Moreover, endothelial metabolism was similarly altered, as higher glycolytic rates were induced by human fibrillar tau compared to control, as measured by extracellular flux analysis at 24 hours after treatment (Figure 6B-C). Western blot analysis of hCMECs treated with human-derived tau fibrils also revealed a dramatic increase in the expression of VCAM-1 (Figure 6D), even more evident than what we had previously observed for the tau protofibrils. Immunocytochemical assessment allowed us to compare cell entry of aggregated protofibrillar 1N4R tau protofibrils and human tau fibrils (Figure 6E). Protofibrillar tau, as previously shown, localized both inside the cell and on the cell membrane, whereas the human-derived tau fibrils appeared to localize preferentially at the cell membrane, although some internalized tau was also observed (Figure 6E). This is likely explained by the more advanced aggregation state and length of these fibrils, which may result in stronger membrane binding, or possibly hinder internalization mechanisms.[42,43] Nevertheless, the loss of barrier function and metabolic alterations seen with more physiologically relevant tau species confirm our previously obtained results.

3.7 | Loss of junction integrity is present in 3-month-old PS19 mouse vessels

The P301S (PS19) mouse model has been widely used for understanding behavioral, neurotoxic, and neuroinflammatory changes caused by the presence of tau pathology, with age-dependent decrease in tau solubility between 3 and 6 months of age and synaptic pathology starting at 3 months. Weak astrogliosis and microglial activation are present in these mice ≈ 3 to 4 months of age,[46] and recent findings point to resting cerebral blood flow decline after 6 months of age.[60] Here, we aimed to determine whether microvascular and BBB pathology and metabolic changes were evident at 3 months of age, when tau fibrils start to be present, but before the onset of tangle pathology. Immunohistochemical analysis of extracted cerebral microvessels of 3-month-old PS19 mice revealed a higher abundance of tau (HT7, green) on capillaries and arterioles (respectively stained by CD31 only, or CD31 and α-SMA) of PS19 mice, compared to WT mice (Figure 7A,B). Moreover, immunohistochemical assessment of junctional proteins ZO-1 (red) and claudin-5 (green; Figure 7C), showed an impaired organization of the tight junctions, as revealed by the decreased colocalization of ZO-1 and claudin-5, measured via Pearson and Manders coefficients (Figure 7D). Line scan analysis of ZO-1 and claudin-5 intensity, with accompanying traces, demonstrates decreased interaction and overlap between the two fluorescent signals at the PS19 vessel junctions (Figure 7E,F).

3.8 | PS19 mice exhibit cerebral microvascular metabolic alterations and pro-inflammatory EC activation at 3 months of age

To assess whether the vascular metabolic alterations observed in vitro in cerebral ECs are also present in this mouse model, we first performed an ATP Production Rate test on extracted WT and PS19 cerebral vessels (Figure 8A, left), which showed increased glycolytic ATP production (Figure 8A, middle) and decreased mitochondrial ATP production (Figure 8A, right), with no changes in total ATP production (Figure S5A in supporting information). Through a Seahorse Mito Stress Test, we then showed that OCRs were decreased in PS19 vessels, resulting in significantly lower basal mitochondrial respiration rate (Figure 8B,C), and apparently reduced (although non-significantly) maximal respiration rate and spare respiratory capacity (Figure S5B). Altered vessel bioenergetics can correlate with overall dysfunction and improper JP maintenance, as well as endothelial inflammatory activation.[26,36] Indeed, western blot analysis revealed increased expression of VCAM-1 in the PS19 cortex (Figure 8D,E), an indication of activated ECs, as also seen in our in vitro model. Further, we observed increased expression of GLUT1, the brain endothelial–specific glucose transporter (Figure 8D–F), correlating with the observed increased in glycolytic rates induced by tau fibrils in ECs (Figure 4), and the increased glycolytic ATP production in microvessels extracted from the PS19 model (Figure 8A, middle). We observed a dramatic increase in both total and cleaved MMP2, the active form responsible for the degradation of the extracellular matrix and basement membrane and known to disrupt JPs (Figure 8D,G), in 3-month-old PS19 mice. We also assessed production in extracted cerebral vessels of cytokines that have been associated with an increased inflammatory and metabolic phenotype. Differently from our in vitro results, we observed no changes in IL-4 production, although this can be due to the presence of other cell types in addition to ECs (pericytes, smooth muscle cells) on the extracted vessels (Figure 8H, far left). We did however observe increased pro-inflammatory cytokines IL-6, Il-5, and IL-1β (Figure 8H, middle left-right). Interestingly we

measurement during mitochondrial stress test indicates increased mitochondrial basal respiration (left), maximal respiration (middle), and ATP production rate (right), with 5 nM protofibrillar tau. F, Immunocytochemical assessment of mitochondrial membrane potential using MitoTracker Red CM-H2XROS. G, Increased expression of mitochondrial superoxide dismutase SOD2 with 5 nM tau, determined by western blot analysis. H, DNA fragmentation in hCMECs after 72 hours of challenge with protofibrillar tau. I, LDH release from hCMECs after 72 hours of challenge with protofibrillar tau. J, Basal respiration rate and ATP production for hCMECs after 72 hours of challenge with protofibrillar tau. K, Glycolytic rates for hCMECs after 72 hours of treatment with protofibrillar tau. Statistical significance was established by one-way analysis of variance; (WB, SH, LDH, and CDE) and Tukey post hoc test. Significant *P* values are reported in the graphs. ATP, adenosine triphosphate; hCMEC, human cerebral microvascular endothelial cell; LDH, lactate dehydrogenase; OCR, oxygen consumption rate; OXPHOS, oxidative hyperphosphorylation; SH, Seahorse; SOD2, superoxide dismutase 2; VCAM-1, vascular cell adhesion molecule 1; WB, western blot.

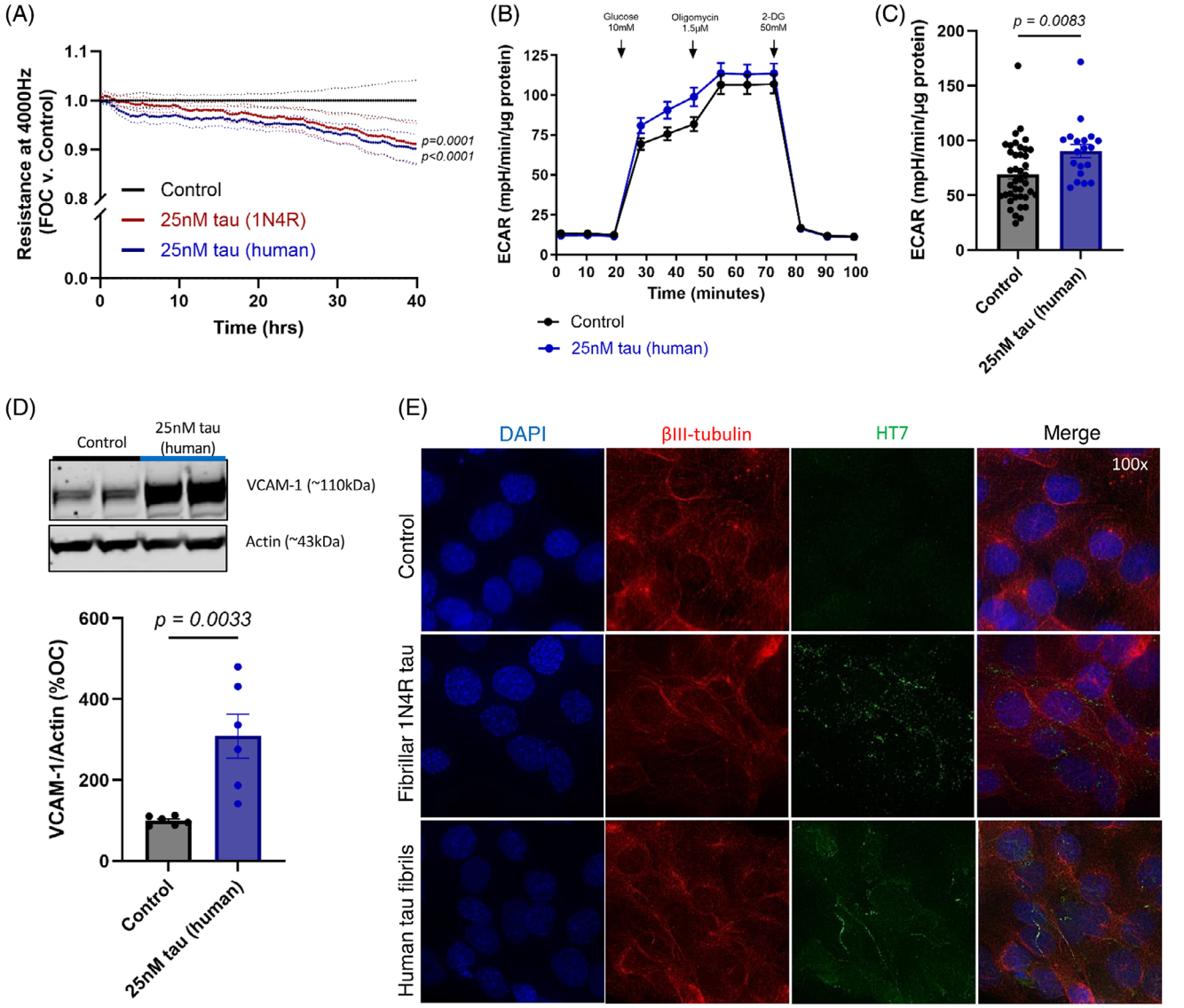

FIGURE 6 Human-derived fibrillar tau induces loss of barrier resistance and pro-inflammatory EC activation. A, TEER trace (at 4000 Hz) of hCMECs treated with 25 nM aggregated 1N4R tau or 25 nM human-derived tau fibrils. B, Representative trace for glycolysis stress test ECAR for hCMECs treated with human-derived fibrillar tau for 24 hours. C, ECAR analysis in hCMECs treated with 25 nM human-derived tau fibrils reveals increased glycolytic rates. D, Western blot analysis of VCAM-1 expression for hCMECs treated with human fibrillar tau (25 nM) for 24 hours. E, Immunocytochemical assessment of protofibrillar 1N4R tau and human-derived tau fibrils on hCMEC monolayers after 24 hours of treatment. Statistical significance established by Student *t* test (WB, SH) and two-way analysis of variance (Electrical Cell Impedance Sensing-Zθ). Significant *P* values are reported in the graphs. EC, endothelial cell; ECAR, extracellular acidification rate; hCMEC, human cerebral microvascular endothelial cell; SH, Seahorse; TEER, trans-endothelial electrical resistance; VCAM-1, vascular cell adhesion molecule 1; WB, western blot.

also observed an increase in IL-10, an anti-inflammatory cytokine (Figure 8H, far right), similarly to our in vitro results (Figure 3G). This suggests an early compensatory protective mechanism activated at the BBB, while reaffirming the notion that early inflammatory events mediated by brain vascular cells are a possible cause for tau-related pathological outcomes in PS19 mice. Overall, our data demonstrate a Warburg-like metabolic switch, with an increase in glycolytic rates and reduction of mitochondrial respiration, in the cerebral vasculature of 3-month-old PS19 mice, an age in which tau fibrillar aggregates, but not tangles, are present. This metabolic switch is associated to endothelial pro-inflammatory phenotype; MMP2 activation; and, based on our experiments on brain ECs, is causal to vascular alterations and neuroinflammation.

4 | DISCUSSION

The presence of tau species in and around the brain vasculature has been recently demonstrated in human AD patients,[14] as well as murine models,[13] suggesting tau aggregates' transmission from neurons or astrocytes, or a failure of aggregated tau clearance at the vessel walls. Moreover, tau depletion was shown to prevent cerebrovascular

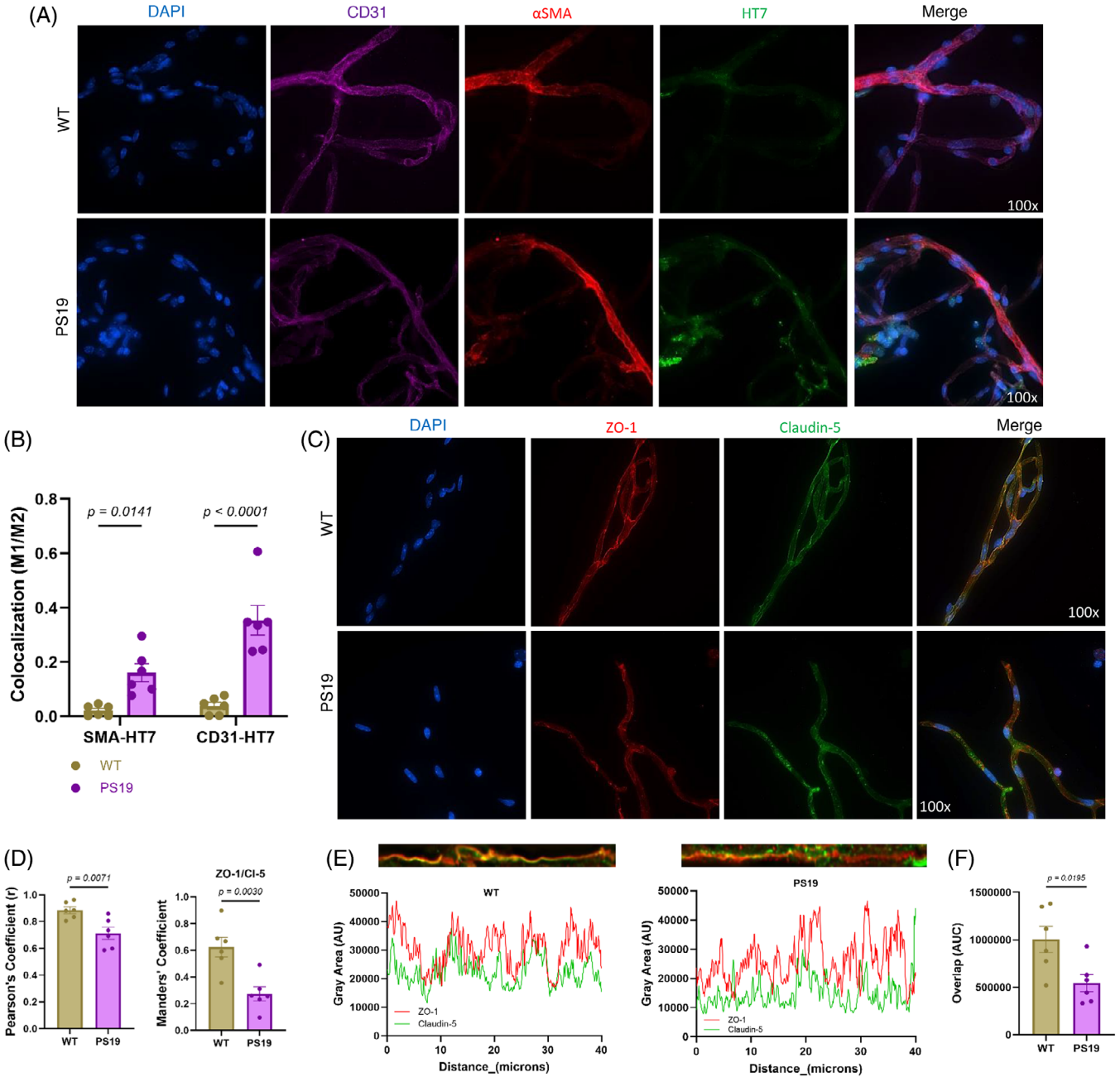

FIGURE 7 Loss of junction integrity in 3-month-old PS19 mice. A, Immunohistochemical assessment of HT7 tau-positive cerebral microvessels, ranging from capillaries to arterioles (determined by αSMA-positive areas). B, Manders coefficient analysis demonstrates higher colocalization of αSMA or CD31 (M1) on HT7 (M2). C, Immunohistochemical assessment of ZO-1 and Claudin-5 on extracted cerebral microvessels from WT and PS19 mice. D, Colocalization measurement of ZO-1 and Claudin-5 fluorescence indicates loss of barrier structure in microvessels of PS19 mice. E, Representative line scan analysis and fluorescence intensity graphs for WT (left) and PS19 mice (right). F, Quantification of area of overlap of the individual line scans. Statistical significance established by two-way analysis of variance; or Student *t* test (colocalization). Significant *P* values are reported in the graphs. WT, wild type.

dysfunction in tauopathy models,[12] highlighting the importance of understanding the possible effects elicited by tau aggregates on the cerebral vasculature. The presence of pathological tau species on ECs, the innermost layer of blood vessels and the site of the BBB, may elicit possible key events for the development of neurovascular alterations in AD, mixed AD/vascular dementias, and other neurodegenerative pathologies. Recent studies have enhanced our understanding of how oligomeric tau damages human cerebral ECs, highlighting the presence of a senescence phenotype after nitric oxide synthase inactivation and microtubule destabilization,[9] a hallmark pathology of aberrant tau. Oligomeric tau has further been shown to disrupt barrier integrity and decrease tight JP expression on mouse cerebral ECs, coupled with induction of oxidative stress,[61] whereas other studies have shown altered cerebrovascular functionality mediated by soluble tau

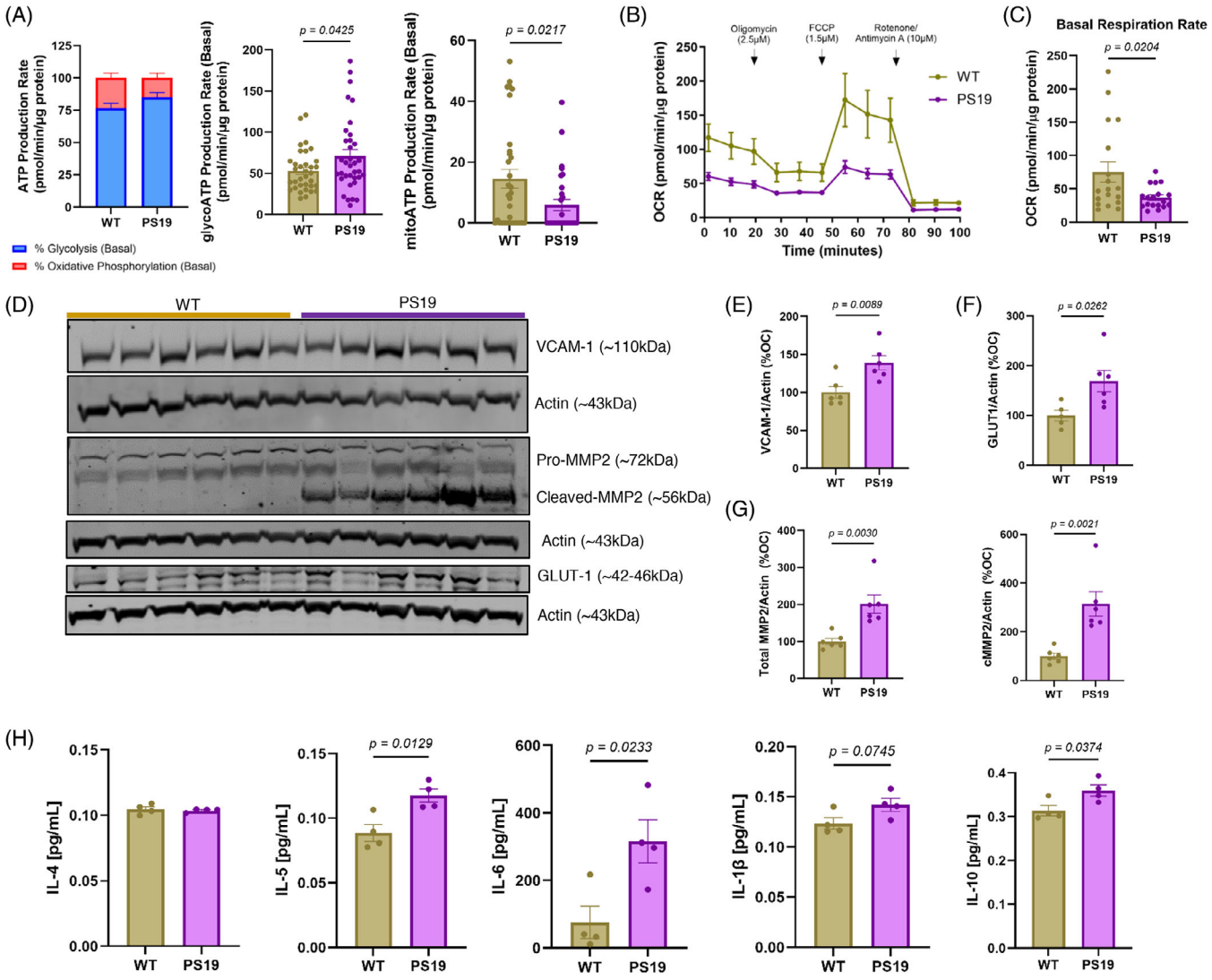

FIGURE 8 PS19 mice demonstrate vascular metabolic dysfunction and EC activation at 3 months. A, ATP production rate assay reveals increased glycolytic ATP production (left) and decreased mitochondrial ATP production rate (middle) in PS19 mice cerebral microvessels, compared to WT mice. Representative ATP production rates by percentage (right). B, Representative trace for Mito Stress Test OCR of extracted vessels reveals deficits in mitochondrial respiratory function in PS19 mice. C, OCR measurement in extracted microvessels demonstrates decreased basal respiration rates in PS19 mice. D–G, Western blot analysis reveals increased VCAM-1 (H) and GLUT1 (I) expression, as well as increases in total (pro-MMP2 + cleaved-MMP2; left) and cleaved (right) MMP2 (J) in PS19 mice cortices. H, Increased pro-inflammatory cytokine production (IL-6, IL-5, IL-1β, and anti-inflammatory cytokine IL-10), by extracted cerebral microvessels. Statistical significance established by Student *t* test (WB, SH, MSD). Significant *p* values or trends are reported in the graphs. ATP, adenosine triphosphate; EC, endothelial cell; IL, interleukin; GLUT1, glucose transporter 1; MMP2, matrix metalloproteinase 2; MSD, Meso Scale Discovery; OCR, oxygen consumption rate; SH, Seahorse; VCAM-1, vascular cell adhesion molecule 1; WB, western blot WT, wild type.

disrupting endothelial calcium signaling and vasodilation.[62] However, it is well known that higher order species of aggregated tau, such as protofibrils or fibrils, can spread throughout the brain. As seen with Aβ in CAA, protofibrillar or fibrillar tau may also deposit at the vessel walls, as a failure of clearance processes or as the endpoint of tau spreading.[14]

Therefore, in the present study, we aimed to elucidate the molecular mechanisms leading to endothelial dysfunction mediated by protofibrillar and fibrillar tau species. We demonstrated that these fibrillar tau species dose-dependently decrease endothelial barrier resistance, rapidly and independently of cell death. Further, they alter JP expression and localization, with early events such as the phosphorylation of VE-Cadherin having a sustained effect on barrier resistance. Tau protofibrils and fibrils also elicit pro-inflammatory activation of ECs, as evidenced by the expression of adhesion molecules such as VCAM-1 and the production and release of pro-inflammatory cytokines, such as IL-4. This activated inflammatory state correlates with metabolic alterations and the early upregulation of glycolytic activity, which is causal to the loss of barrier functionality. After longer treatment times, cell death pathways are also initiated, coinciding with a failure of

mitochondrial respiration. These results were further corroborated using human brain-derived tau fibrils, as well as in the P301S model of tauopathy, in which we observed vascular deposition of tau, loss of JP localization, and increased endothelial glycolytic and inflammatory activity, with reduced mitochondrial respiration, at 3 months of age, a time point preceding widespread tangle pathology and neuronal loss.

Our interest in the effects of protofibrillar and fibrillar tau species on barrier resistance stems from the need to understand how different tau aggregates may contribute to BBB damage. Recently, oligomeric tau has been shown to decrease TEER and JP expression[63] in mouse CECs. However, the effects of protofibrillar or fibrillar tau on the BBB were not yet known.

Tau species participate in pro-inflammatory pathways,[18] including NLRP3 inflammasome activation;[64,65] activation of microglia via the cGAS-STING pathway;[66,67] and, most recently, oligomeric tau has been shown to activate ECs through the Rho/ROCK pathway.[61] Our results demonstrate that fibrillar and protofibrillar tau induce pro-inflammatory activation of human cerebral ECs and the upregulation of molecules that mediate the adhesion and entry of immune cells in the brain. Particularly, an overexpression of VCAM-1 at the vessel lumen is known to mediate leukocyte rolling, thus increasing BBB permeability.[68,69] We hypothesized that increased endothelial cytokine production may be responsible for these effects. Interestingly, our results indicate that fibrillar tau does not induce EC release of classical pro-inflammatory cytokines, such as IL-1β, Il-6, and IL-8. We did however observe an early overproduction of TNF-α and IFN-γ, while IL-4 upregulation was observed early and also maintained at later time points. IL-4 has been shown to mediate VCAM-1 upregulation[70] and endothelial permeability.[55] In our model, IL-4 blockade only partially prevented tau-mediated BBB permeability; yet inhibition of glycolysis was sufficient to completely prevent barrier permeability and the increase in VCAM-1 induced by fibrillar tau, suggesting that glycolytic changes are causal for reduced barrier resistance and EC activation. Interestingly, recent findings in peripheral and brain ECs have similarly shown that the activation of glycolytic pathways mediates endothelial inflammatory activation.[26,30,34–37]

Dysregulation of glucose metabolism is one of the key pathologies present in AD, as shown across recent studies.[71,72] Our results highlight a previously undiscovered increase in glycolytic rates in ECs treated with tau protofibrils, which appears to mediate an EC pro-inflammatory activation that ultimately leads to loss of barrier resistance. This phenomenon is already present at early treatment time points, and its inhibition prevents barrier permeability, indicating that the increase in glycolysis is possibly required to sustain the observed pro-inflammatory phenotype and mediate barrier permeability.[36,73] Importantly, we confirmed a similar metabolic alteration in vessels extracted from 3-month-old PS19 mice, where we observed a Warburg-like increase in glycolytic ATP production and a decrease in mitochondrial respiration. The increase in glycolysis was accompanied by an increase in pro-inflammatory vascular markers, such as VCAM-1 and MMP2, and an increase in GLUT1, the major endothelial glucose transporter, in the brain of PS19 mice, confirming an increased need for glucose to perform glycolysis.

Notably, although peripheral ECs are primarily glycolytic, brain ECs are more dependent on mitochondrial metabolism and have a higher number of mitochondria,[74] further suggesting that an increase in glycolysis in brain ECs may be maladaptive, associated to a cerebral EC reversal to a state more similar to peripheral ECs and to the loss of BBB function. In line with the observed changes, tau has been previously shown to interact with mitochondrial compartments, including in cerebral ECs[75,76] and with glycolytic enzymes, namely, GAPDH,[77] highlighting the importance of considering metabolic and mitochondrial alterations as early or causal events in the context of AD and tauopathies.

Overall, this study has shown previously undiscovered effects of protofibrillar and fibrillar tau on EC metabolism, linking an early tau-induced metabolic stress response and increased glycolysis to pro-inflammatory EC activation, loss of healthy tight junctions, and impaired BBB resistance. We also observed that chronic exposure to tau protofibrils resulted in reduction of endothelial mitochondrial respiration and, eventually, apoptotic cell death. Further, we confirmed the loss of mitochondrial respiration and increased glycolytic ATP production in vessels extracted from 3-month-old PS19 mice, accompanied by endothelial activation and neurovascular dysfunction markers in PS19 mouse brains. Using both in vitro and in vivo models of tauopathy, we shed light on the molecular mechanisms and metabolic changes through which fibrillar tau species mediate loss of barrier resistance and damage the endothelial barrier, increasing barrier permeability and endothelial inflammatory activation.

This study also has some limitations: more research is needed to understand the early events that lead to the altered metabolic phenotype elicited by tau aggregates on the brain vasculature. It also remains to be assessed whether tau oligomers induce similar metabolic and inflammatory stress pathways associated to BBB dysfunction. We did not perform in vivo measurements of barrier permeability, cerebral blood flow, or behavioral assessments in the tauopathy mice; however, these are reported in great detail elsewhere.[9,60] Further, in our experiments with human-derived tau fibrils, we observed a stronger presence of tau on the cell membrane, rather than internalized, compared to synthetic aggregated tau protofibrils. While this may be due to the human-derived fibrils being longer and more aggregated, the dramatic increase in VCAM expression triggered by the human-derived fibrils highlights the possibility of a membrane receptor–mediated signaling leading to the observed endothelial proinflammatory phenotype. This remains to be addressed through future studies, currently under development by our group. Additionally, other molecular pathways and parallel stress responses elicited by aggregated tau in ECs may contribute to cerebrovascular dysfunction, warranting further investigations.

5 | CONCLUSION

This research provides a needed understanding of the detrimental effects of tau fibrillar aggregates on EC metabolism, inflammatory activation, and BBB function in vitro and in vivo, uncovering novel

molecular mechanisms and metabolic changes that may explain tau-mediated cerebrovascular dysfunction outcomes, and highlighting potential targets for therapeutic interventions against neurovascular pathology in AD, tauopathies, and mixed AD/vascular dementias.

AUTHOR CONTRIBUTIONS

Silvia Fossati and Roberto Guzmán-Hernández designed and conceptualized the study, and wrote and revised the manuscript. Roberto Guzmán-Hernández performed experiments and statistical analysis. Silvia Fossati acquired funding.

ACKNOWLEDGMENTS

Electron microscopy was performed at the MitoCare Service Center (Thomas Jefferson University, Philadelphia, PA, USA). We thank Dr. Rakez Kayed for generously sharing the human-tau derived fibrils. This work was supported by NIH R01NS104127 (NINDS) and R01AG062572 (NIA) grants, and the Pennsylvania Department of Health Collaborative Research on Alzheimer's Disease (PA Cure) Grant, awarded to S.F.

CONFLICT OF INTEREST STATEMENT

The authors declare no conflicts of interest. Author disclosures are available in the supporting information.

CONSENT STATEMENT

No human samples were used in the presented results; therefore, consent was not necessary for this study.

REFERENCES

1. Hachinski V, Einhäupl K, Ganten D, et al. Preventing dementia by preventing stroke: the Berlin Manifesto. *Alzheimers Dement*. 2019;15(7):961-984.
2. Iturria-Medina Y, Sotero RC, Toussaint PJ, et al. Early role of vascular dysregulation on late-onset Alzheimer's disease based on multifactorial data-driven analysis. *Nat Commun*. 2016;7:11934.
3. Schaeffer S, Iadecola C. Revisiting the neurovascular unit. *Nat Neurosci*. 2021;24(9):1198-1209.
4. Parodi-Rullán RM, Javadov S, Fossati S. Dissecting the crosstalk between endothelial mitochondrial damage, vascular inflammation, and neurodegeneration in cerebral amyloid angiopathy and Alzheimer's disease. *Cells*. 2021;10(11):2903.
5. Parodi-Rullán R, Ghiso J, Cabrera E, Rostagno A, Fossati S. Alzheimer's amyloid beta heterogeneous species differentially affect brain endothelial cell viability, blood-brain barrier integrity, and angiogenesis. *Aging Cell*. 2020;19(11):e13258.
6. Parodi-Rullán R, Sone JY, Fossati S. Endothelial mitochondrial dysfunction in cerebral amyloid angiopathy and Alzheimer's disease. *J Alzheimers Dis*. 2019;72(4):1019-1039.
7. Ghiso J, Fossati S, Rostagno A. Amyloidosis associated with cerebral amyloid angiopathy: cell signaling pathways elicited in cerebral endothelial cells. *J Alzheimers Dis*. 2014;42(0):S167-S176.
8. Canepa E, Fossati S. Impact of tau on neurovascular pathology in Alzheimer's disease. *Front Neurol*. 2020;11:573324.
9. Hussong SA, Banh AQ, Van Skike CE, et al. Soluble pathogenic tau enters brain vascular endothelial cells and drives cellular senescence and brain microvascular dysfunction in a mouse model of tauopathy. *Nat Commun*. 2023;14(1):2367.
10. Michalicova A, Majerova P, Kovac A. Tau protein and its role in blood-brain barrier dysfunction. *Front Mol Neurosci*. 2020;13:570045.
11. Bennett RE, Robbins AB, Hu M, et al. Tau induces blood vessel abnormalities and angiogenesis-related gene expression in P301L transgenic mice and human Alzheimer's disease. *Proc Natl Acad Sci USA*. 2018;115(6):E1289-E1298.
12. Blair LJ, Frauen HD, Zhang B, et al. Tau depletion prevents progressive blood-brain barrier damage in a mouse model of tauopathy. *Acta Neuropathol Commun*. 2015;3:8.
13. Castillo-Carranza DL, Nilson AN, Van Skike CE, et al. Cerebral microvascular accumulation of tau oligomers in Alzheimer's disease and related tauopathies. *Aging Dis*. 2017;8(3):257-266.
14. Hoglund Z, Ruiz-Uribe N, del Sastre E, et al. Brain vasculature accumulates tau and is spatially related to tau tangle pathology in Alzheimer's disease. *Acta Neuropathol*. 2024;147(1):101.
15. Tagge CA, Fisher AM, Minaeva OV, et al. Concussion, microvascular injury, and early tauopathy in young athletes after impact head injury and an impact concussion mouse model. *Brain*. 2018;141(2):422-458.
16. Kirsch D, Shah A, Dixon E, et al. Vascular injury is associated with repetitive head impacts and tau pathology in chronic traumatic encephalopathy. *J Neuropathol Exp Neurol*. 2023;82(2):127-139.
17. McKee AC, Stein TD, Nowinski CJ, et al. The spectrum of disease in chronic traumatic encephalopathy. *Brain*. 2013;136(Pt 1):43-64.
18. Nilson AN, English KC, Gerson JE, et al. Tau oligomers associate with inflammation in the brain and retina of tauopathy mice and in neurodegenerative diseases. *J Alzheimers Dis*. 2017;55(3):1083-1099.
19. Gibbons G, Lee V, Trojanowski J. Mechanisms of cell-to-cell transmission of pathological tau: a review. *JAMA Neurol*. 2019;76(1):101-108.
20. Uemura N, Uemura MT, Luk KC, Lee VM, Trojanowski JQ. Cell-to-cell transmission of tau and alpha-synuclein. *Trends Mol Med*. 2020;26(10):936-952.
21. Kim Y, Park H, Kim Y, et al. Pathogenic role of RAGE in tau transmission and memory deficits. *Biol Psychiatry*. 2023;93(9):829-841.
22. Iba M, Guo JL, McBride JD, Zhang B, Trojanowski JQ, Lee VM. Synthetic tau fibrils mediate transmission of neurofibrillary tangles in a transgenic mouse model of Alzheimer's-like tauopathy. *J Neurosci*. 2013;33(3):1024-1037.
23. Evans LD, Wassmer T, Fraser G, et al. Extracellular monomeric and aggregated tau efficiently enter human neurons through overlapping but distinct pathways. *Cell Rep*. 2018;22(13):3612-3624.
24. Cooper JM, Lathuiliere A, Migliorini M, et al. Regulation of tau internalization, degradation, and seeding by LRP1 reveals multiple pathways for tau catabolism. *J Biol Chem*. 2021;296:100715.
25. Rauch JN, Luna G, Guzman E, et al. LRP1 is a master regulator of tau uptake and spread. *Nature*. 2020;580(7803):381-385.
26. Xiao W, Oldham WM, Priolo C, Pandey AK, Loscalzo J. Immunometabolic endothelial phenotypes: integrating inflammation and glucose metabolism. *Circ Res*. 2021;129(1):9-29.
27. Berndt P, Winkler L, Cording J, et al. Tight junction proteins at the blood-brain barrier: far more than claudin-5. *Cell Mol Life Sci*. 2019;76(10):1987-2002.
28. Yazdani S, Jaldin-Fincati JR, Pereira RVS, Klip A. Endothelial cell barriers: transport of molecules between blood and tissues. *Traffic*. 2019;20(6):390-403.
29. Kluge M, Fetterman J, Vita J. Mitochondria and endothelial function. *Circ Res*. 2013;112(8):1171-1188.
30. McDonald C, Blankenheim Z, Drewes L. Brain endothelial cells: metabolic flux and energy metabolism. *Handb Exp Pharmacol*. 2022;273:59-79.
31. Tang X, Luo Y, Chen H, Liu D. Mitochondria, endothelial cell function, and vascular diseases. *Front Physiol*. 2014;5:175.
32. Caja S, Enríquez JA. Mitochondria in endothelial cells: sensors and integrators of environmental cues. *Redox Biol*. 2017;12:821-827.

33. Marcu R, Kotha S, Zhi Z, et al. The mitochondrial permeability transition pore regulates endothelial bioenergetics and angiogenesis. *Circ Res*. 2015;116(8):1336-1345.
34. Yang K, Fan M, Wang X, et al. Lactate induces vascular permeability via disruption of VE-cadherin in endothelial cells during sepsis. *Sci Adv*. 2022;8(17):eabm8965.
35. Leung S, Shi Y. The glycolytic process in endothelial cells and its implications. *Acta Pharmacol Sin*. 2022;43(2):251-259.
36. Kim ES, Kim K, Lee CH, et al. Brain endothelial cells utilize glycolysis for the maintenance of the transcellular permeability. *Mol Neurobiol*. 2022;59(7):4315-4333.
37. Schnitzler JG, Hoogeveen RM, Ali L, et al. Atherogenic lipoprotein(a) increases vascular glycolysis, thereby facilitating inflammation and leukocyte extravasation. *Circ Res*. 2020;126(10):1346-1359.
38. Estudillo E, López-Ornelas A, Rodríguez-Oviedo A, Gutiérrez de la Cruz N, Vargas-Hernández MA, Jiménez A. Thinking outside the black box: are the brain endothelial cells the new main target in Alzheimer's disease? *Neural Regen Res*. 2023;18(12):2592-2598.
39. Oliveri D, Moschetti G, Griego A, Scarpa E. Endothelial cellular senescence and tau accumulation: an interplay full of opportunities? *Ibrain*. 2024;10(2):225-230.
40. Tarawneh R. Microvascular contributions to Alzheimer disease pathogenesis: is Alzheimer disease primarily an endotheliopathy? *Biomolecules*. 2023;13(5):830.
41. Mutreja Y, Gamblin T. Optimization of in vitro conditions to study the arachidonic acid induction of 4R isoforms of the microtubule-associated protein tau. *Methods Cell Biol*. 2017;141:65-88.
42. Tarutani A, Lövestam S, Zhang X, et al. Cryo-EM structures of tau filaments from SH-SY5Y cells seeded with brain extracts from cases of Alzheimer's disease and corticobasal degeneration. *FEBS Open Bio*. 2023;13(8):1394-1404.
43. Lovestam S, Koh FA, van Knippenberg B, et al. Assembly of recombinant tau into filaments identical to those of Alzheimer's disease and chronic traumatic encephalopathy. *Elife*. 2022;11:e76494.
44. Weksler BB, Subileau EA, Perrière N, et al. Blood-brain barrier-specific properties of a human adult brain endothelial cell line. *FASEB J*. 2005;19(13):1872-1874.
45. Carey A, Parodi-Rullan R, Vazquez-Torres R, Canepa E, Fossati S. Homocysteine potentiates amyloid beta -induced death receptor 4- and 5-mediated cerebral endothelial cell apoptosis, blood brain barrier dysfunction and angiogenic impairment. *Aging Cell*. 2024; 23: e14106.
46. Yoshiyama Y, Higuchi M, Zhang B, et al. Synapse loss and microglial activation precede tangles in a P301S tauopathy mouse model. *Neuron*. 2007;53(3):337-351.
47. Lee Y, Uchida H, Smith H, Ito A, Sanchez T. The isolation and molecular characterization of cerebral microvessels. *Nat Protoc*. 2019;14(11):3059-3081.
48. Sure VN, Sakamuri SSVP, Sperling JA, et al. A novel high-throughput assay for respiration in isolated brain microvessels reveals impaired mitochondrial function in the aged mice. *Geroscience*. 2018;40(4):365-375.
49. Brunello CA, Merezhko M, Uronen R, Huttunen HJ. Mechanisms of secretion and spreading of pathological tau protein. *Cell Mol Life Sci*. 2020;77(9):1721-1744.
50. Kelly L, Brown C, Michalik D, et al. Clearance of interstitial fluid (ISF) and CSF (CLIC) group-part of vascular professional interest area (PIA), updates in 2022-2023. Cerebrovascular disease and the failure of elimination of Amyloid-beta from the brain and retina with age and Alzheimer's disease: opportunities for therapy. *Alzheimers Dement*. 2023;20(2):1421-1435.
51. Caughey B, Lansbury P. Protofibrils, pores, fibrils, and neurodegeneration: separating the responsible protein aggregates from the innocent bystanders. *Annu Rev Neurosci*. 2003;26:267-298.
52. Walsh DM, Hartley DM, Kusumoto Y, et al. Amyloid beta-protein fibrillogenesis. structure and biological activity of protofibrillar intermediates. *J Biol Chem*. 1999;274(36):25945-25952.
53. Grammas P, Martinez J, Miller B. Cerebral microvascular endothelium and the pathogenesis of neurodegenerative diseases. *Expert Rev Mol Med*. 2011;13:e19.
54. Soto-Heredero G, Gómez de las Heras MM, Gabandé-Rodríguez E, Oller J, Mittelbrunn M. Glycolysis—a key player in the inflammatory response. *FEBS J*. 2020;287(16):3350-3369.
55. Skaria T, Burgener J, Bachli E, Schoedon G. IL-4 causes hyperpermeability of vascular endothelial cells through Wnt5A signaling. *PLoS One*. 2016;11(5):e0156002.
56. Zhang L, Wang Z, Yuan X, Sui R, Falahati M. Evaluation of heptelidic acid as a potential inhibitor for tau aggregation-induced Alzheimer's disease and associated neurotoxicity. *Int J Biol Macromol*. 2021;183:1155-1161.
57. Kushnareva Y, Newmeyer D. Bioenergetics and cell death. *Ann N Y Acad Sci*. 2010;1201:50-57.
58. Nicotera P, Leist M, Fava E, Berliocchi L, Volbracht C. Energy requirement for caspase activation and neuronal cell death. *Brain Pathol*. 2000;10(2):276-282.
59. Chidambaram SB, Anand N, Varma SR, et al. Superoxide dismutase and neurological disorders. *IBRO Neurosci Rep*. 2024;16:373-394.
60. Ahmad F, Mein H, Jing Y, Zhang H, Liu P. Behavioural functions and cerebral blood flow in a P301S tauopathy mouse model: a time-course study. *Int J Mol Sci*. 2021;22(18):9727.
61. Hossen F, Sun G, Lee J. Oligomeric tau-induced oxidative damage and functional alterations in cerebral endothelial cells: role of RhoA/ROCK signaling pathway. *Free Radic Biol Med*. 2024;221:261-272.
62. Mughal A, Sackheim AM, Koide M, et al. Pathogenic soluble tau peptide disrupts endothelial calcium signaling and vasodilation in the brain microvasculature. *J Cereb Blood Flow Metab*. 2024;44(5):680-688.
63. Hossen F, Geng X, Sun GY, Yao X, Lee JC. Oligomeric amyloid-beta and tau alter cell adhesion properties and induce inflammatory responses in cerebral endothelial cells through the RhoA/ROCK pathway. *Mol Neurobiol*. 2024;61(11):8759-8776.
64. de Oliveira P, Cella C, Locker N, et al. Improved sleep, memory, and cellular pathological features of tauopathy, including the NLRP3 inflammasome, after chronic administration of trazodone in rTg4510 mice. *J Neurosci*. 2022;42(16):3494-3509.
65. Ising C, Venegas C, Zhang S, et al. NLRP3 inflammasome activation drives tau pathology. *Nature*. 2019;575(7784):669-673.
66. Jin M, Shiwaku H, Tanaka H, et al. Tau activates microglia via the PQBP1-cGAS-STING pathway to promote brain inflammation. *Nat Commun*. 2021;12(1):6565.
67. Carling GK, Fan L, Foxe NR, et al. Alzheimer's disease-linked risk alleles elevate microglial cGAS-associated senescence and neurodegeneration in a tauopathy model. *Neuron*. 2024;112(23):3877-3896.e8.
68. Zhang H, Shang J, Li W, Gao D, Zhang J. Increased expression of VCAM1 on brain endothelial cells drives blood-brain barrier impairment following chronic cerebral hypoperfusion. *ACS Chem Neurosci*. 2024;15(10):2028-2041.
69. Cook-Mills J. VCAM-1 signals during lymphocyte migration: role of reactive oxygen species. *Mol Immunol*. 2002;39(9):499-508.
70. Lee YW, Kühn H, Hennig B, Neish AS, Toborek M. IL-4-induced oxidative stress upregulates VCAM-1 gene expression in human endothelial cells. *J Mol Cell Cardiol*. 2001;33(1):83-94.
71. Liu Y, Liu F, Iqbal K, Grundke-Iqbal I, Gong C. Decreased glucose transporters correlate to abnormal hyperphosphorylation of tau in Alzheimer disease. *FEBS Lett*. 2008;582(2):359-364.
72. Minhas PS, Jones JR, Latif-Hernandez A, et al. Restoring hippocampal glucose metabolism rescues cognition across Alzheimer's disease pathologies. *Science*. 2024;385(6711):eabm6131.

73. Salmina AB, Kuvacheva NV, Morgun AV, et al. Glycolysis-mediated control of blood-brain barrier development and function. *Int J Biochem Cell Biol*. 2015;64:174-184.
74. Oldendorf W, Cornford M, Brown W. The large apparent work capability of the blood-brain barrier: a study of the mitochondrial content of capillary endothelial cells in brain and other tissues of the rat. *Ann Neurol*. 1977;1(5):409-417.
75. Rabanal-Ruiz Y, Pedrero-Prieto C, Sanchez-Rodriguez L, et al. Differential accumulation of human beta-amyloid and tau from enriched extracts in neuronal and endothelial cells. *Biochim Biophys Acta Mol Basis Dis*. 2024;1870(5):167204.
76. Tracy TE, Madero-Pérez J, Swaney DL, et al. Tau interactome maps synaptic and mitochondrial processes associated with neurodegeneration. *Cell*. 2022;185(4):712-728. e14.
77. Wang Q, Woltjer RL, Cimino PJ, et al. Proteomic analysis of neurofibrillary tangles in Alzheimer disease identifies GAPDH as a detergent-insoluble paired helical filament tau binding protein. *FASEB J*. 2005;19(7):869-871.

SUPPORTING INFORMATION

Additional supporting information can be found online in the Supporting Information section at the end of this article.

How to cite this article: Guzmán-Hernández R, Fossati S. Fibrillar tau alters cerebral endothelial cell metabolism, vascular inflammatory activation, and barrier function in vitro and in vivo. *Alzheimer's Dement*. 2025;21:e70077. https://doi.org/10.1002/alz.70077